

Relaminarization of Moderate Turbulent Pipe Flow via Axial Rotation

---

DISSERTATION

---

A dissertation submitted in partial  
fulfillment of the requirements for the  
degree of Master of Science in the College  
of Engineering at the University of  
Kentucky

By  
Michael Raba  
Lexington, Kentucky

Director: Dr. Christoph Brehm,  
Department of Aerospace Engineering  
University of Maryland, College Park  
College Park, Maryland  
2024

Copyright<sup>©</sup> Michael Raba 2024  
<https://orcid.org/0009-0009-4444-562X>

## ABSTRACT OF DISSERTATION

### Relaminarization of Moderate Turbulent Pipe Flow via Axial Rotation

In previous studies, encompassing simulations and theoretical analysis, the influence of rotation has been significantly observed in altering the dynamics of turbulent flows. Notably, it can modify the mean velocity profile to resemble that of laminar flow, contributing to a reduction in drag. It also impacts the Reynolds stress tensor. An archetypal example of such complex turbulent flow phenomena is observed in an axially rotating pipe. In this scenario, pipe rotation induces a zone of turbulence suppression, which is notably sensitive to both the rotation rate and the Reynolds number,  $Re$ . The underlying physical mechanisms responsible for this turbulence suppression remain largely elusive. However, comprehending these mechanisms is crucial for various practical applications involving swirling or rotating flows, like swirl generators, wing-tip vortices, and axial compressors.

In this research, Direct Numerical Simulations (DNS) of rotating turbulent pipe flows are executed at moderate Reynolds numbers ( $Re = 5300$  and  $11700$ ) and rotation numbers ( $S = \{0, 0.5, 1, 3\}$ ). The primary goals of this study are to quantify the extent of turbulence suppression in rotating turbulent pipe flows across different Reynolds numbers, and to examine the impact of rotation on turbulence. This is achieved by analyzing the characteristics of the Reynolds stress tensor, alongside the production and dissipation terms within the turbulence budgets.

KEYWORDS: Proper Orthogonal Decomposition, Relaminarization, Turbulent Flow

---

Michael Raba

---

May 4, 2024

Relaminarization of Moderate Turbulent Pipe Flow via Axial Rotation

By  
Michael Raba

---

Dr. Christoph Brehm  
Director of Dissertation

---

Dr. Jonathan Wenk  
Director of Graduate Studies

---

May 4, 2024  
Date



## ACKNOWLEDGMENTS

I would like to thank my advisor Christoph Brehm for taking me on as a student - without his trust, this project would not have been a success.

I would like to also thank Dr Alex Martin for his support throughout the MSc process, Dr Sean Bailey for discussions above turbulence theory, Dr Steven Brunton of the University of Washington for POD questions early on in the project, and Dr Oliver Browne with getting me involved with the CFD lab.

I would like to thank Sparsh Ganju and Bijaylakshmi Saikia for early work in getting setup with the project.

I would like to thank Pum Thian Lal Neihguk, my friend and classmate, for frequent discussions on POD, but also engineering as a profession and guidance.

I would like to thank my parents, Timothy and Tammy, for their support and love, and my brothers and sisters, Jaime, Jonathan, Nicholas, Emily, Anne, Kimberly, Virginia, Rebecca, and Molly.

## TABLE OF CONTENTS

Acknowledgments . . . . .	i
List of Tables . . . . .	iii
List of Figures . . . . .	iv
Chapter 1 Introduction . . . . .	1
1.0.1 Motivation and Goals . . . . .	1
1.0.2 Relaminarization and Rotating Pipe Flows . . . . .	1
1.0.3 Proper Orthogonal Decomposition . . . . .	2
1.0.4 Coherent Structure Forms . . . . .	2
1.0.5 Turbulence Statistics . . . . .	2
Chapter 2 Method Spectral-Element Direct Numerical Solution (DNS) . . . . .	3
2.0.1 Simulation Setup of Spectral Element Method . . . . .	3
2.0.2 Governing Equations of Motion . . . . .	3
2.0.3 Mesh Details and Simulation Setup details . . . . .	4
Chapter 3 Theory . . . . .	7
3.0.1 Snapshot Proper Orthogonal Decompositon . . . . .	7
3.0.2 Classical Proper Orthogonal Decompositon . . . . .	9
Chapter 4 Rotating Pipe POD Results . . . . .	11
4.0.1 Producing POD modes $\Phi(r; m)$ in practice . . . . .	11
4.0.2 Results — Two Dimensional POD Projection Validation . . . . .	11
4.0.3 Radial Modal Results and Comparison with Published Literature . . . . .	14
4.0.4 Most Dominant Modes . . . . .	17
4.0.5 Turbulent Statistics . . . . .	18
4.0.6 Reconstruction . . . . .	19
Chapter 5 Appendix to: Rotating Pipe POD Results . . . . .	21
5.1 POD Mode Projections . . . . .	21
Chapter 6 Summary, Discussion, and Conclusions . . . . .	35
6.0.1 Coherent Structures . . . . .	37
6.0.2 Rotating Pipes . . . . .	37
6.0.3 Turbulent Flows . . . . .	38
6.0.4 Classical POD . . . . .	39
6.0.5 Spectral Analysis . . . . .	39
6.0.6 NEK5000 . . . . .	40

## LIST OF TABLES

2.1 Grid spacings, measured in $y^+$ units, for a streamwise extent of 15 diameters, where the grid is non-uniform, and denser close to the wall. . . . .	4
-----------------------------------------------------------------------------------------------------------------------------------------------------------	---

## LIST OF FIGURES

2.1 Non-Uniform mesh employed for Spectral Element Method DNS. . . . .	4
2.2 Uniform, interpolated mesh with interpolation factor of 4, which is used for POD analysis . . .	5
4.1 Comparison of the POD mode from the instantaneous flowfield from Hellström, Marusic, and Smits [34]. This demonstates that, for a subset of instantaneous snapshots of the flowfield, it's POD projection captures the essential features. In this figure, the POD has 5 light and dark lobes, and the flowfield has, albeit in some less clear way, 5 light spots and 5 dark spots, representing the 5th azimuthal mode is likely to have a large eigenvalue as well, in comparsion to the total energy. . . . .	12
4.2 (top) The modal profiles of the streamwise component $\langle \phi^{(2)} \rangle$ for $S = 3.0$ . . . . .	13
4.3 (top) The modal profiles of the streamwise component $\langle \phi^{(3)} \rangle$ for $S = 3.0$ . . . . .	14
4.4 (top) The modal profiles of the streamwise component $\langle \phi^{(4)} \rangle$ for $S = 3.0$ . . . . .	15
4.5 Derivation of POD projections . . . . .	16
4.6 Arbitrary POD mode (here pictured: $(n, m) = (12, 5)$ with $S = 3$ ) is $C^\infty$ . No windowing has been applied, and for most modes whose 2D POD projections are converged, no spectral leakage is present. . . . .	17
4.7 (top) The modal profiles of the streamwise component $\langle \phi^{(1)} \rangle$ for $S = 0.0$ . The modal profiles show the energy content in relation to the pipe wall $r = 0$ . (bottom) Contour plots of the streamwise components of sample POD modes for $m = \{5, 10, \dots, 30\}$ for $n = 1$ . Note that since these modes are converged, and those we are then able to recover the modal profiles shown at (top). . . . .	19
4.8 Reconstruction of a snapshot using 400 POD modes and 50 azimuthal modes. . . . .	20

## Chapter 1

### Introduction

#### 1.0.1 Motivation and Goals

This thesis covers turbulent flow in rotating pipes. Flow in pipes is a type of wall-bounded flows, which are confined to a (curved) wall, and are responsible for interesting physics, since the pipe wall introduces no-slip condition. Turbulence has been studied in the past, in terms of turbulent energy and energy cascades, starting with Kolmogorov [44].

A goal of this thesis is to study turbulence through the lens of coherent structures. A coherent structure refers to a region within a fluid flow where the patterns of flow velocity, vorticity (rotation), or other flow properties exhibit a consistent and identifiable pattern or structure over a certain scale of space or time. They carry the bulk of energy, and provide an explanation for how energy is transported.

A second goal of this thesis is to study how the turbulent flow can be relaminarized. This is the process whereby a fluid becomes less turbulent. This has been achieved in the past via either active or passive flow control. In this study, it is via rotation at different swirl rates  $S$ . Previous studies, such as Kikuyama et al. [42] identified different effects of pipe rotation on the flow stability, momentum transport, and aligned reynolds stress tensors: they identified that a flow may be both destabilized (by the large shear at the pipe wall) and stabilized (by the center rotating core's centrifugal force).

#### 1.0.2 Relaminarization and Rotating Pipe Flows

The turbulent flow in a rotating pipe serves as an exemplary case to explore the mechanisms leading to relaminarization in rotating flows. While models like RANS and wall-resolved LES fall short in accurately capturing the intricacies of turbulence suppression, DNS emerges as a potent tool to investigate the effects of rotation on turbulent structures, especially near boundary layers, where DNS is able to precisely capture the flow physics. In terms of validating the flow physics of this work, one may consult the comparison of several RANS models with the DNS data presented in this study by Ashton, Davis, and Brehm [3]. In fact, the simulations used in this thesis were produced by (Davis, Brehm, Ganju) during the Spring 2019 and published in a conference paper Brehm et al. [14] (Southampton looks like). In general, previous DNS studies on rotating pipe flows have been limited to relatively lower Reynolds numbers, displaying a pronounced dependence on the rotation number. Therefore, this study aims to provide comprehensive DNS data at higher Reynolds numbers.

Pioneering experiments on rotating pipe flow by White [85] observed a pressure loss reduction of up to 40% at high rotation numbers, attributing this to diminished radial transport. Kikuyama et al. (1983) noted that sufficiently high rotation numbers could seemingly relaminarize an initially turbulent flow, while initially laminar flows became destabilized. Imao, Itoh, and Harada [40] confirmed a decrease in turbulence intensity with increasing rotation rates, establishing a link between reduced mixing length and the Richardson number. More recently, Facciolo et al. (2007) found their mean velocity distribution data to align well with scaling laws derived by Oberlack [60] using the Lie group method, as presented in Oberlack [59] for high-Re rotating and non-rotating turbulent pipe flows.

Comparatively, rotating circular pipe flow has been less explored numerically than the (spanwise) rotating channel flow. Previous DNS studies, conducted for  $Re \leq 7,400$  and generally at lower  $N$ , have indicated some form of turbulence suppression, albeit not complete relaminarization. The extensive DNS studies by Orlandi and Fatica [61], which explored rotation numbers up to  $N = 2$  at  $Re = 4,900$  (and later up to  $N = 10$  in Orlandi and Ebstein [63]), revealed a form of relaminarization that remains poorly understood. In this relaminarization, the mean streamwise velocity profile converges towards the laminar Poiseuille profile.

While Nishibori, Kikuyama, and Murakami [57] and Reich and Beer [69] attributed the observed changes to centrifugal forces, Orlandi & Fatica (1997) suggested modifications in near-wall flow structures as the cause. Their simulations qualitatively mirrored the drag and turbulence reductions seen in experiments but with some discrepancies, potentially due to uncertainties in experimental flow conditions and measurement locations.

Feiz, Ould-Rouis, and Lauriat [24] undertook DNS for fully developed turbulent flows in both stationary and axially rotating pipes. Their study varied Reynolds numbers, considering  $Re = 4,900$  and  $Re = 7,400$ , along with rotation numbers up to  $N = 2$ . They noted that the axial mean velocity profiles at  $Re = 7,400$  were lower than those at  $Re = 4,900$ . The tangential mean velocity profiles appeared similar for both Reynolds numbers. Additionally, their LES at  $Re = 20,000$  showed a more pronounced decrease in skin friction factor with increasing  $N$  for higher  $Re$ .

This thesis will proceed as follows: Chapter 2 offers an overview of the simulation setup and numerical approach. The theory of POD is discussed in Chapter 3; the results of the POD and the resulting coherent structures are discussed in Chapter 4; results such as effects of rotation on turbulent mean flow shall also be included in the future. Also to be added are eigenvalue chart ranking the POD and azimuthal modes relative contribution, and Conditional POD modes shall be given. In Chapter 4 Appendix color plate of the 2d POD projections are given. In the future, a further chapter, Chapter 5 shall quantify turbulence suppression in rotating flows - it is necessary because it is the goal of this thesis. In that chapter modifications in the Reynolds stress tensor structure shall be examined, and finally, the analysis of the production and dissipation terms will shed light on the mechanisms behind turbulence suppression in rotating flow.

### 1.0.3 Proper Orthogonal Decomposition

The POD, also known as the Karhunen-Loëve expansion, was initially introduced in the field of hydrodynamics to define coherent structures in turbulence Lumley [49].

The idea behind POD is to project high-dimensional data onto a lower-dimensional space using an orthogonal basis, which captures the dominant modes of variation in the data. The basis is obtained by performing a Singular Value Decomposition (SVD) on the data matrix, which decomposes it into three matrices - a left singular matrix, a diagonal singular value matrix, and a right singular matrix. The left and right singular matrices contain the left and right eigenvectors of the covariance matrix of the data, respectively, while the singular values represent the variance of the data along these eigenvectors.

The resulting basis functions can be used to reconstruct the original data with minimal loss of information, as they capture the dominant patterns of variability in the data Taira et al. [80]. This can be particularly useful in situations where the original data is high-dimensional and noisy, making it difficult to extract meaningful information from the raw data.

### 1.0.4 Coherent Structure Forms

A subsection discussing different forms such as hairpin, horse shoe, may be discussed, especially if carpet plots are included in subsequent chapters.

### 1.0.5 Turbulence Statistics

A subsection discussing turbulent statistics shall be added. This is needed for discussing Reynolds stress.

## Chapter 2

### Method Spectral-Element Direct Numerical Solution (DNS)

#### 2.0.1 Simulation Setup of Spectral Element Method

A circular pipe with dimensionless diameter ( $D = 1$ ) and length ( $L = 12D$ ) is selected as the computation domain to conduct the DNS of internal pipe turbulent flow. The dimensionless INS equations are solved with  $Re = \{5300, 12700\}$ . Non-slip boundary condition is used at the wall, with periodical boundary condition at the in- and outlet at both ends.

Under the spectral element method, Legendre basis functions are used to solve the velocity space. Inside each element, the solution has a Legendre polynomial order ( $lx1$ ) equal to 6, which is equivalent to distributing 5 nodes in each direction of the element. The mesh with  $lx1 = 6$  is shown. Since we are interested to show the flow behavior near the pipe wall at Kolmogorov and Taylor scales, and to find the reduced order models which are accurate near the wall, the non-uniform mesh has been chosen such that it is finer near the wall.

#### 2.0.2 Governing Equations of Motion

The governing equations implemented in Nek5000 are the dimensionless incompressible Navier-Stokes (NSE) equations as shown,

$$\nabla \cdot \mathbf{u} = 0 \frac{\partial \mathbf{u}}{\partial t} + (\mathbf{u} \cdot \nabla) \quad (2.1)$$

$$\mathbf{u} = -\nabla p + \frac{1}{Re} \nabla^2 u, \quad (2.2)$$

where  $(u, p)$  is the velocity vector and pressure and  $Re$  is the Reynolds number,

$$Re = \frac{\rho U D_h}{\mu}, \quad \text{Swirl Number } S = \frac{V_w}{U_b} \quad (2.3)$$

and where  $\rho$  is the density,  $U$  is the characteristic velocity,  $U_b$  is the bulk velocity,  $D_h$  is the hydraulic diameter, and  $\mu$  is the dynamic viscosity. This can be written in cylindrical coordinates (reference:Kundu, Cohen, and Dowling [45]) as,

$$\frac{\partial w}{\partial t} + w \frac{\partial w}{\partial r} + \frac{v}{r} \frac{\partial w}{\partial \theta} + u \frac{\partial w}{\partial x} - \frac{v^2}{r} = \quad (2.4)$$

$$-\frac{1}{\rho} \frac{\partial p}{\partial r} + \nu \left( \mathcal{D}w - \frac{w}{r^2} - \frac{2}{r^2} \frac{\partial v}{\partial \theta} \right) - 2\Omega v \quad (2.5)$$

$$(2.6)$$

$$\frac{\partial v}{\partial t} + w \frac{\partial v}{\partial r} + \frac{vw}{r} + \frac{v}{r} \frac{\partial v}{\partial \theta} + u \frac{\partial v}{\partial x} = \quad (2.7)$$

$$-\frac{1}{\rho r} \frac{\partial p}{\partial \theta} + \nu \left( \mathcal{D}v - \frac{v}{r^2} + \frac{2}{r^2} \frac{\partial w}{\partial \theta} \right) + 2\Omega w \quad (2.8)$$

$$(2.9)$$

$$\frac{\partial u}{\partial t} + w \frac{\partial u}{\partial r} + \frac{v}{r} \frac{\partial u}{\partial \theta} + u \frac{\partial u}{\partial x} = \quad (2.10)$$

$$-\frac{1}{\rho} \frac{\partial p}{\partial x} + \nu \mathcal{D}u \quad (2.11)$$

where

$$\mathcal{D} = \frac{\partial^2}{\partial r^2} + \frac{1}{r} \frac{\partial}{\partial r} + \frac{1}{r^2} \frac{\partial^2}{\partial \theta^2} + \frac{\partial^2}{\partial x^2} \quad (2.12)$$

The boundary conditions on the pipe wall are in laboratory reference frame (not rotating with the pipe), for  $S > 0$ , are given by

$$u_r(R) = 0, u_\theta(R) = \Omega R, u_x(R) = 0 \text{ where the rotation vector is } \Omega = \Omega e_k \quad (2.13)$$

and it is assumed the flow is incompressible, and the pipe wall is smooth.

### 2.0.3 Mesh Details and Simulation Setup details

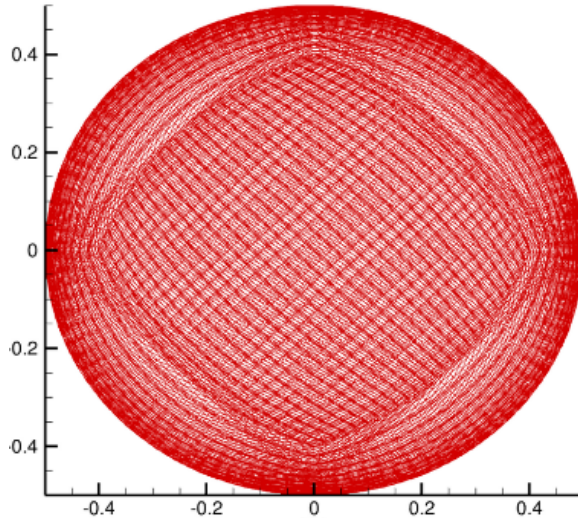


Figure 2.1: Non-Uniform mesh employed for Spectral Element Method DNS.

Table 2.1: Grid spacings, measured in  $y^+$  units, for a streamwise extent of 15 diameters, where the grid is non-uniform, and denser close to the wall.

$Re$	$\Delta r^+ / \Delta R \Theta^+ / \Delta z^+$	$N_{\Delta t} 10^6$
5,300	0.14-4/1.5 -4.5/ 3.0-9.9	20
11,700	0.15-4.5/1.5-4.8/3.0-10	120

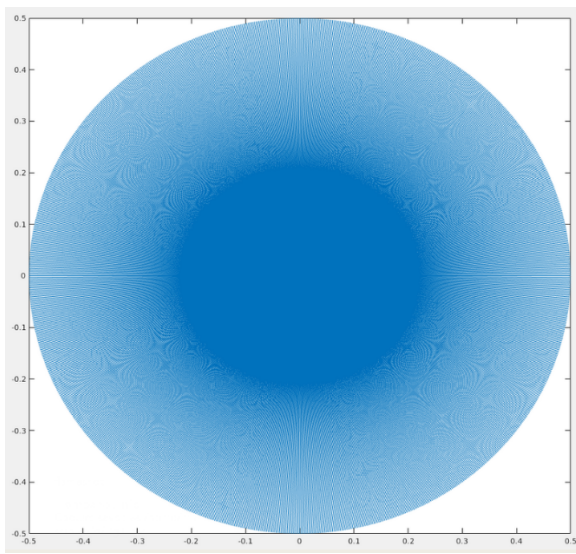


Figure 2.2: Uniform, interpolated mesh with interpolation factor of 4, which is used for POD analysis



## Chapter 3

### Theory

We use proper orthogonal decomposition (POD) to decompose the turbulent fluctuating velocity flow field to a reduced order model (ROM): POD provides a method that is both representative of the original flow field and sparse; it is the orthogonality property of POD that allows us to do this Taira et al. [80].

There are related forms of POD, classical and snapshot variants. Snapshot POD forms a covariance matrix in terms of time, whereas the former it is in terms of spatial extent. We choose snapshot as Taira notes it converges vastly more quicker. Without convergence, the radial turbulent profiles will not be able to be found. In fact, we are able to find highly converged profiles, as we do in the sequel Chapter 4.

In fact, we are performing hybrid fft-POD approach in this study. We are decomposing  $u'$  in  $\theta$  direction in terms of Fourier modes. This is because the flow field is periodic in  $\theta$ , and fourier modes can capture this without information loss. We also can decompose  $u'$  in the streamwise direction ( $x$ ), which is also periodic, by construction of the simulation's periodic boundary condition. (see: recycled flow diagram Davis Bailey Brehm Ashton 2018 paper and the above chapter on simulation setup). However, it was found that Fourier transform in  $x$ -direction was superfluous since the profiles are streamwise invariant.

Next, we need to decompose in the radial direction: since  $u'$  in *not* periodic in  $r$ , we cannot use Fourier modes to capture the flow statistic. Instead we use POD, whose basis elements  $\phi^i$  are bespoke to the (non-periodic) flow data. The snapshot POD basis elements are dense, so that we need very few basis elements to capture the flow behavior. In Chapter 4, we will show the turbulent flow for different swirl numbers  $S$  may be accurately described by only 3 or 4 POD modes  $n$ , and a few azimuthal modes  $m$ .

In writing out the fft-POD, it is important to be mindful of its mathematical form and meaning. It is an integral equation of the first kind, whose solution is guaranteed to exist by functional analysis existence theorem (Hilbert-Smidt theory).

Next, it is important to exploit the POD modes periodicity in the  $x$  direction. The eigenvalues are unique up to the  $\pm$  sign. We can average the crosssections along  $x$  to represent the POD decomposition without loss of information.

Finally, we are interested in the near wall behavior of the flow. Rather than taking  $\hat{f}_\theta$  for each  $x$ , this step can be done on the ensemble  $\langle u\alpha^*(r, \theta) \rangle$ .

#### 3.0.1 Snapshot Proper Orthogonal Decompositon

Each snapshot of the stochastic process in contained in a Hilbert space equiped with an inner product

$$\langle q_1, q_2 \rangle_{r,t} = \int q_1 q_2^* r dr dt \quad (3.1)$$

where  $q_1(r_1, t_1)$  and  $q_2(r_1, t_2)$  are two snapshots of the flow. We then maximalize the projection coefficient,  $\lambda$ , which represents the energy (Lumley 1967), given by

$$\lambda = \frac{E\{|q(r, t), \Phi(r, t)|^2\}}{\langle (r, t)\Phi(r, t) \rangle_{r,t}} \quad (3.2)$$

which leads (explain) to

$$\int R(t, t') \Phi(t') dt = \lambda \Phi(t) \quad (3.3)$$

where  $R(t, t') = E\{q(r, t)q^*(r, t')\}$  is the two point time correlation tensor. Moreover we are assuming that as  $T \rightarrow \infty$  the system reaches steady state, so the system is elliptic, so the eigenvalue problem may be fairly posed.

We start with the direct POD equation, where the cross-correlation tensor depends on the azimuthal mode number, streamwise wavenumber and the radial two-point correlation represented by  $r$  and  $r'$ . The eigenvalue problem becomes

$$\int_{r'} \mathbf{S}(k; m; r, r') \Phi^{(n)}(k; m; r') r' dr' = \lambda^{(n)}(k; m) \Phi^{(n)}(k; m; r), \quad (3.4)$$

where  $n$  represents the POD mode number,  $\Phi^{(n)}$  are the radial eigenfunctions with the corresponding eigenvalues  $\lambda^{(n)}$ , and there exist a set of  $(n)$  radial modes for each azimuthal and streamwise mode number combination. The time-averaged cross-correlation tensor,  $\mathbf{S}$ , is defined as

$$\mathbf{S}(k; m; r, r') = \lim_{\tau \rightarrow \infty} \frac{1}{\tau} \int_0^\tau \mathbf{u}(k; m; r, t) \mathbf{u}^*(k; m; r', t) dt \quad (3.5)$$

where  $\mathbf{u}$  represents the three-component velocity field, and  $*$  is its conjugate transpose. The method of snapshots assumes that the flow is separable in time and space, which can be written as

$$\alpha^{(n)}(k; m; t) = \int_r \mathbf{u}(k; m; r, t) \Phi^{(n)*}(k; m; r) r dr \quad (3.6)$$

To derive the questioned equation, consider the integral:

$$\frac{1}{\tau} \int_0^\tau \mathbf{u}_T(k; m; r, t) \alpha^{(n)*}(k; m; t) dt. \quad (3.7)$$

Substitute  $\mathbf{u}_T$  with its expansion:

$$\frac{1}{\tau} \int_0^\tau \left( \sum_l \Phi_T^{(l)}(k; m; r) \alpha^{(l)}(k; m; t) \right) \alpha^{(n)*}(k; m; t) dt. \quad (3.8)$$

Exchange the order of summation and integration, and apply orthogonality,

$$\sum_l \Phi_T^{(l)}(k; m; r) \left( \frac{1}{\tau} \int_0^\tau \alpha^{(l)}(k; m; t) \alpha^{(n)*}(k; m; t) dt \right). \quad (3.9)$$

Due to the orthogonality, all terms where  $l \neq n$  will vanish, and there remains only the  $l = n$  term,

$$\Phi_T^{(n)}(k; m; r) \left( \frac{1}{\tau} \int_0^\tau \alpha^{(n)}(k; m; t) \alpha^{(n)*}(k; m; t) dt \right). \quad (3.10)$$

Assuming  $\alpha^{(n)}(k; m; t)$  are normalized or that the integration yields a factor that can be absorbed into  $\Phi_T^{(n)}$ , this simplifies to,

$$\Phi_T^{(n)}(k; m; r) \lambda^{(n)}(k; m), \quad (3.11)$$

where the factor  $\lambda^{(n)}(k; m)$  represents the eigenvalue associated with the  $\alpha^{(n)}$  mode, reflecting its contribution or scaling in the system dynamics.

This derivation assumes the normalization of modes and their orthogonality, along with the eigenvalue relationship to simplify the original integral into a form that reveals the spatial structure ( $\Phi_T^{(n)}$ ) of each mode scaled by its significance ( $\lambda^{(n)}$ ).

The eigenvalue problem can now be rewritten to identify the POD coefficients  $\alpha^{(n)}$ ,

$$\lim_{\tau \rightarrow \infty} \frac{1}{\tau} \int_0^\tau \mathbf{R}(k; m; t, t') \alpha^{(n)}(k; m; t') dt' = \lambda^{(n)}(k; m) \alpha^{(n)}(k; m; t) \quad (3.12)$$

The cross-correlation tensor  $\mathbf{R}$  is defined as  $\mathbf{R}(k; m; t, t') = \int_r \mathbf{u}(k; m; r, t) \mathbf{u}^*(k; m; r, t') r dr$ . This tensor is now transformed from  $[3r \times 3r']$  to a  $[t \times t']$  tensor. The  $n$  POD modes are then constructed as,

$$\lim_{\tau \rightarrow \infty} \frac{1}{\tau} \int_0^\tau \mathbf{u}_T(k; m; r, t) \alpha^{(n)*}(k; m; t) dt = \Phi_T^{(n)}(k; m; r) \lambda^{(n)}(k; m). \quad (3.13)$$

### 3.0.2 Classical Proper Orthogonal Decompositon

We may instead form the correlation tensor  $S(r, r')$ ,

$$\int_{r'} \mathbf{S}(k; m; r, r') \Phi^{(n)}(k; m; r') r' dr' = \lambda^{(n)}(k; m) \Phi^{(n)}(k; m; r), \quad (3.14)$$

as done in eg Tutkun George 2001, and Hellstrom Smits 2014. The correlation tensor is not Hermitian in  $r$ , which is a requirement for existence of the solution  $\Phi$  for Fredholm integral equations of the first type (source), but can be made as such by writing

$$\underbrace{\int_{r'} r'^{1/2} S_{i,j}(r, r'; m; f) r'^{1/2} \underbrace{\phi_j^{*(n)}(r'; m; f) r'^{1/2}}_{\hat{\phi}_j^{\psi(i)}(r'; m; f)} dr'}_{W_{i,j}(r, r'; m; f)} = \underbrace{\lambda^{(n)}(m, f)}_{\hat{\lambda}^{(n)}(m; f)} \underbrace{r^{1/2} \phi_i^{(n)}(r; m; f)}_{\hat{\phi}_i^{(n)}(r, m; f)} \quad (3.15)$$

so that the integral equation is given by

$$\lim_{\tau \rightarrow \infty} \frac{1}{\tau} \int_0^\tau \left( r^{1/2} \mathbf{u}(m; r, t), r^{1/2} \mathbf{u}(m; r, t') \right) \alpha_n(m; t) dt' = \lambda_n(m) \alpha_n(m; t), \quad (3.16)$$

and the time coefficient is

$$\alpha_n(m; t) = \int_r \mathbf{u}(m; r, t) r^{1/2} \Phi_n^*(m; r) dr \quad (3.17)$$



## Chapter 4

### Rotating Pipe POD Results

This chapter presents the results of the theory as presented in Chapter 3. It seeks to validate the POD against especially Hellström, Marusic, and Smits [34] and Hellström and Smits [37] as benchmarks for POD pipe DNS study with no swirl. No valid studies have been published as of this writing on POD with rotating pipes. The below results are in agreement with other studies, which while do not study POD, discuss energy in bulk, in particular its transfer away from the pipe wall Kikuyama et al. [42].

#### 4.0.1 Producing POD modes $\Phi(r; m)$ in practice

Observing the two-dimensional POD projections, it has is observed that for azimuthal modes  $m \in [0, 30]$ , the snapshot POD modes converge for  $m \in [1, 30]$  readily according to the following procedure: since the POD projection is unique only up to  $\pm 1$ , the 2D modes can be correlated for all  $x_i$  so that they are flipped the same direction. It was observed that the POD projections may be averaged in this direction, and the resulting eigenface appears symmetrical in some sense in the azimuthal direction for any given azimuthal and POD mode number pair  $(m, n)$ . This is also true for rotating pipe cases ( $S = 0.5, 1, 3$ ) — see 4.2. Thus the modes are invariant in the streamwise direction  $x$ , as also found in Hellström, Marusic, and Smits [34] and Hellström and Smits [37]. These 2D projections are the starting point for getting radial modal profiles. It is noted that without first finding the averaged 2D POD projection, it is often not possible to accurately derive a radial modal profile.

The one-dimensional model profiles  $\Phi(r; m)$  can be found by taking the FFT of the averaged POD 2d projection in the  $\theta$ -direction:

$$\Phi_T^{(n)}(k; m; r) \lambda^{(n)}(m) = \left\langle \lim_{\tau \rightarrow \infty} \frac{1}{\tau} \int_0^\tau \mathbf{u}_T(k; m; r, t) \alpha^{(n)*}(k; m; t) dt \right\rangle \quad (4.1)$$

$$= \mathcal{F}_\theta \left( \lim_{\tau \rightarrow \infty} \frac{1}{N} \sum_k^N \frac{1}{\tau} \int_0^\tau \mathbf{u}_T(k; \theta; r, t) \alpha^{(n)*}(k; m; t) dt \right) \quad (4.2)$$

= (Fourier transform in azimuthal direction of phase-shifted eigenface) (4.3)

The result is a circular crosssection that is almost everywhere constant - there are two lines which appear to be differentially continuous  $\Phi(r; m) \in C^\infty$ . The radial modal profiles occur twice, owing to the double sidedness of the Fourier transform, and the location of each line is offset by one azimuthal angle (a azimuthal mode  $m$  occurs at  $m - 1$  and  $3m$  number of total angles —  $m + 1$ ). This modal profile is displayed in 4.5 and represents the  $m^{th}$  azimuthal mode of the  $n$ -th order POD. The units are in terms of wall units, so that the interval  $[0, 1]$  represents the distance from pipe wall to the center, and the amplitude  $\langle \Phi(r; m) \rangle_x$  is in terms of energy.

#### 4.0.2 Results — Two Dimensional POD Projection Validation

In terms validation of the foregoing results, the 2D POD projections represent accurately the eddy ensemble, so the POD modes can be compared with instantaneous snapshots. In Hellström, Marusic, and Smits [34], the authors select snapshots such that the magnitude of the POD coefficient  $\alpha^{(1)}$  is larger than twice its root mean square value. Then, they were able to validate that the 2D mode was indeed representative in some sense. Similarly, we can see from 4.0.2 that the POD has no sense of “swirl” for  $S = 0$ , whereas for  $S = 3$  the 2D Mode accurately captures the swirling flow field.

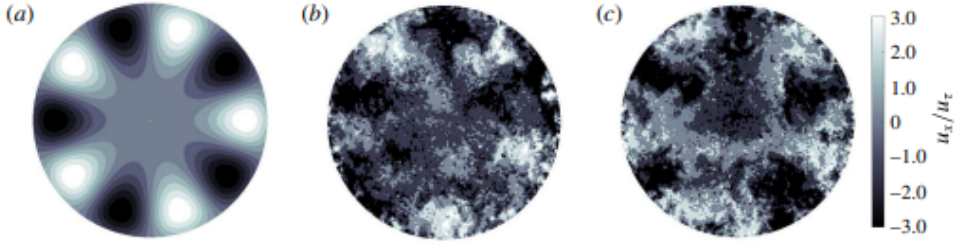
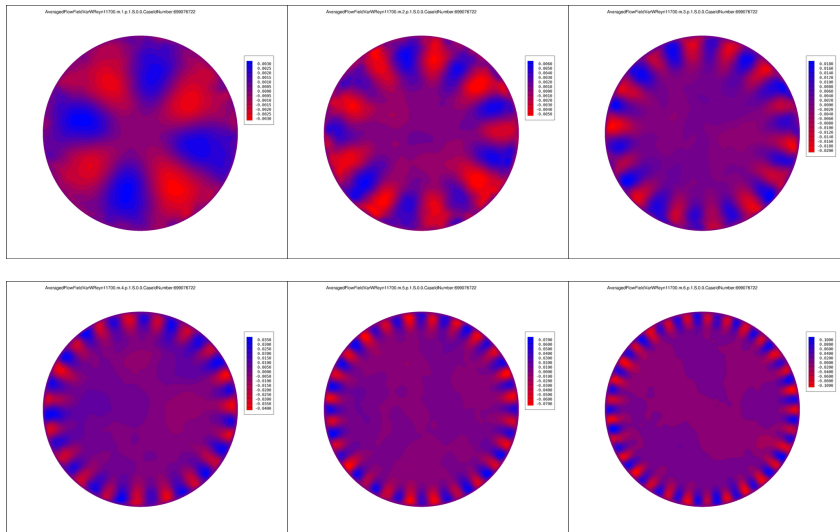
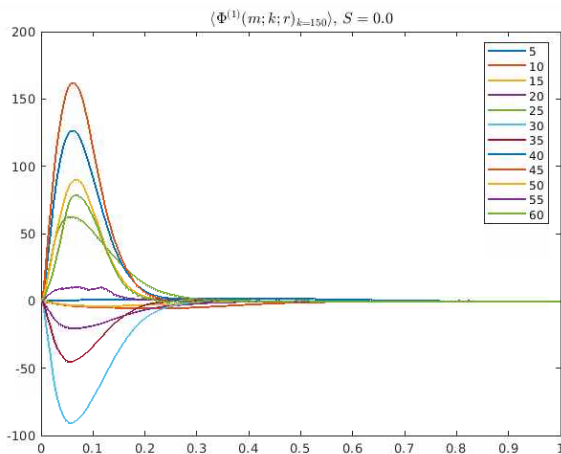


Figure 4.1: Comparison of the POD mode from the instantaneous flowfield from Hellström, Marusic, and Smits [34]. This demonstrates that, for a subset of instantaneous snapshots of the flowfield, its POD projection captures the essential features. In this figure, the POD has 5 light and dark lobes, and the flowfield has, albeit in some less clear way, 5 light spots and 5 dark spots, representing the 5th azimuthal mode is likely to have a large eigenvalue as well, in comparison to the total energy.



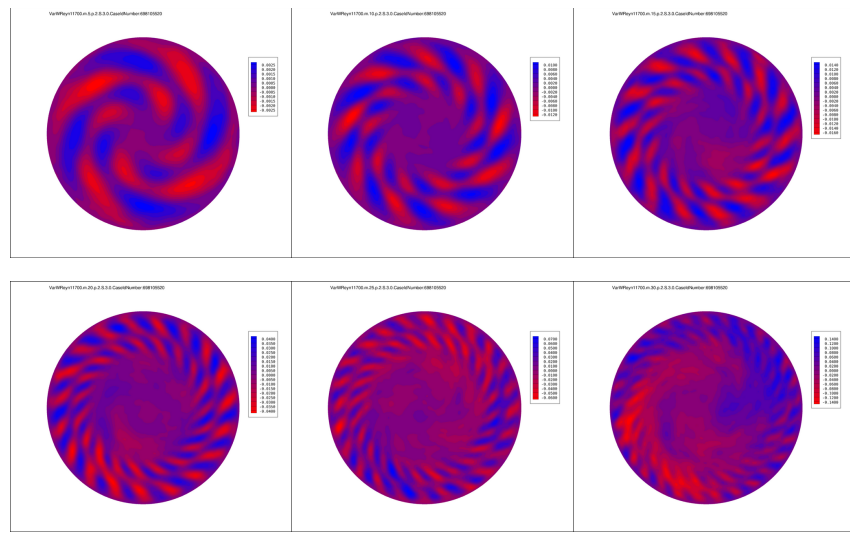
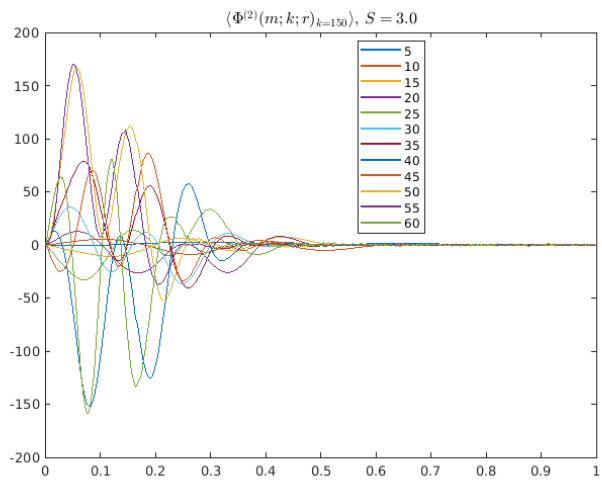


Figure 4.2: (top) The modal profiles of the streamwise component  $\langle \phi^{(2)} \rangle$  for  $S = 3.0$

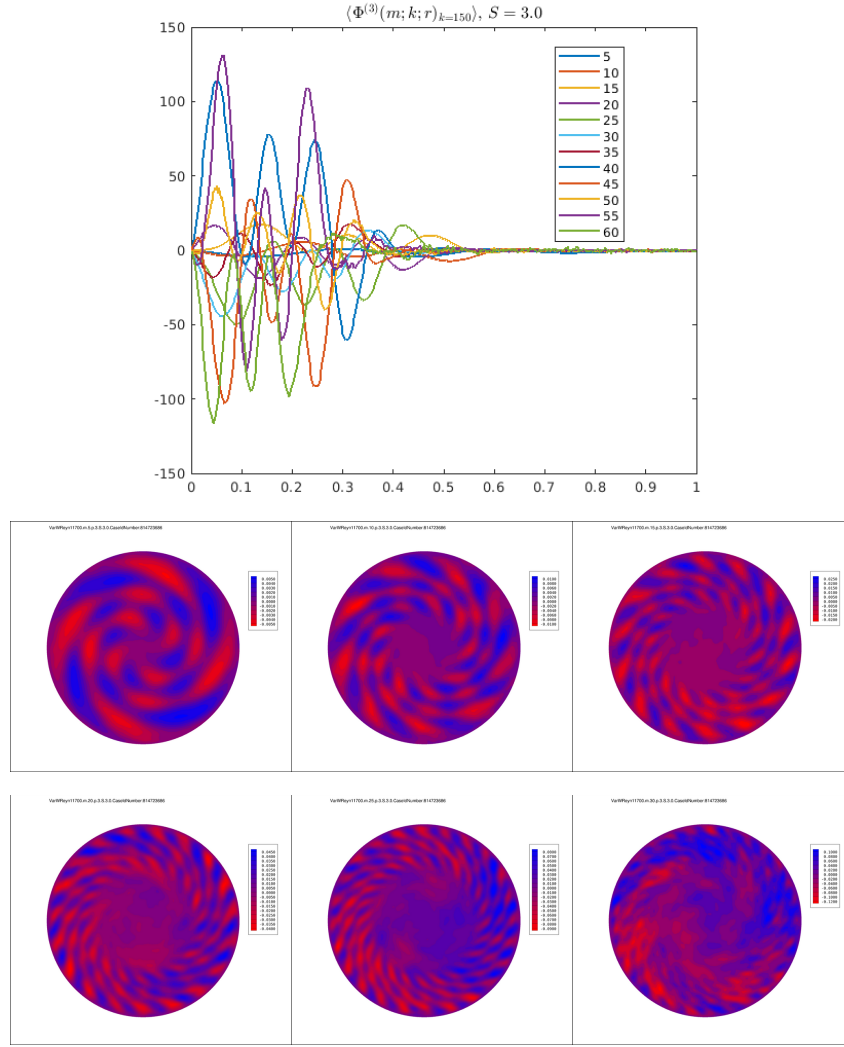


Figure 4.3: (top) The modal profiles of the streamwise component  $\langle \phi^{(3)} \rangle$  for  $S = 3.0$

#### 4.0.3 Radial Modal Results and Comparison with Published Literature

To validate the radial model profile, we compare the no-swirl  $S = 0$  case with Hellström, Marusic, and Smits [34] and Hellström and Smits [37]. First, the computed profiles appear to be  $C^\infty$  for all calculated POD numbers, azimuthal modes  $m$ , and swirl numbers  $S$ , see a closeup view of this in figure.

Second, the modes are orthogonal for each  $m$ , values of  $\Phi(r; k)$  have been normalized by the radially-weighted norm  $\|\Phi\| = \left(\int_0^R \Phi^2(r)r dr\right)^{1/2}$ .

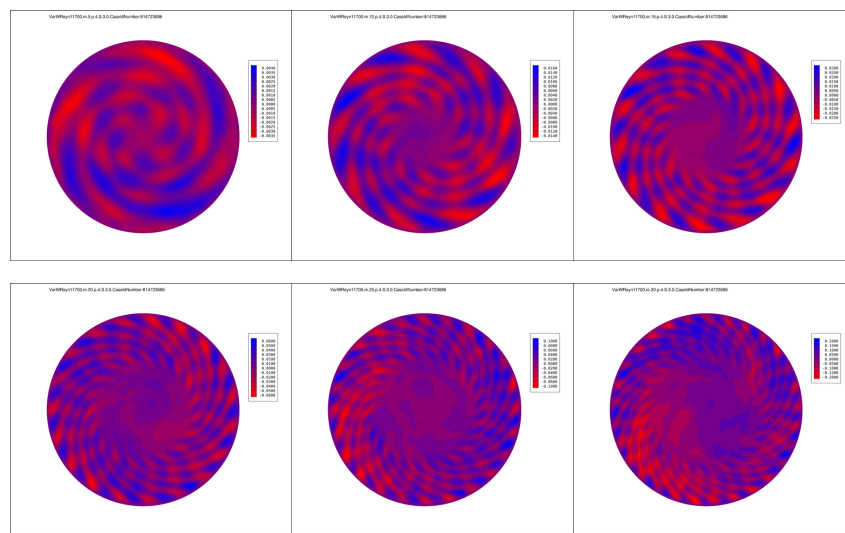
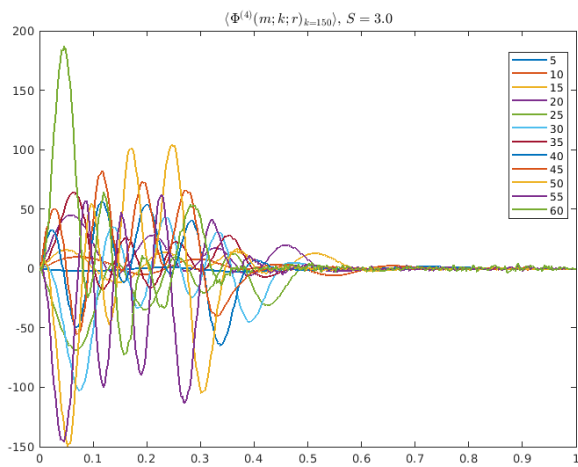


Figure 4.4: (top) The modal profiles of the streamwise component  $\langle \phi^{(4)} \rangle$  for  $S = 3.0$

Figure. The following steps show how to pragmatically find model profiles: after find the two-dimensional projection  $\langle u(r, \theta, t) \alpha^*(t, m, k) \rangle_k$ , the FFT is taken in the azimuthal direction  $\theta$ . Owing to the double sidedness of FFT, two lines are apparent on 2d graph (top right) and shown in three dimensional view (bottom left). These lines are the POD modal profiles and are  $C^\infty$  functions.

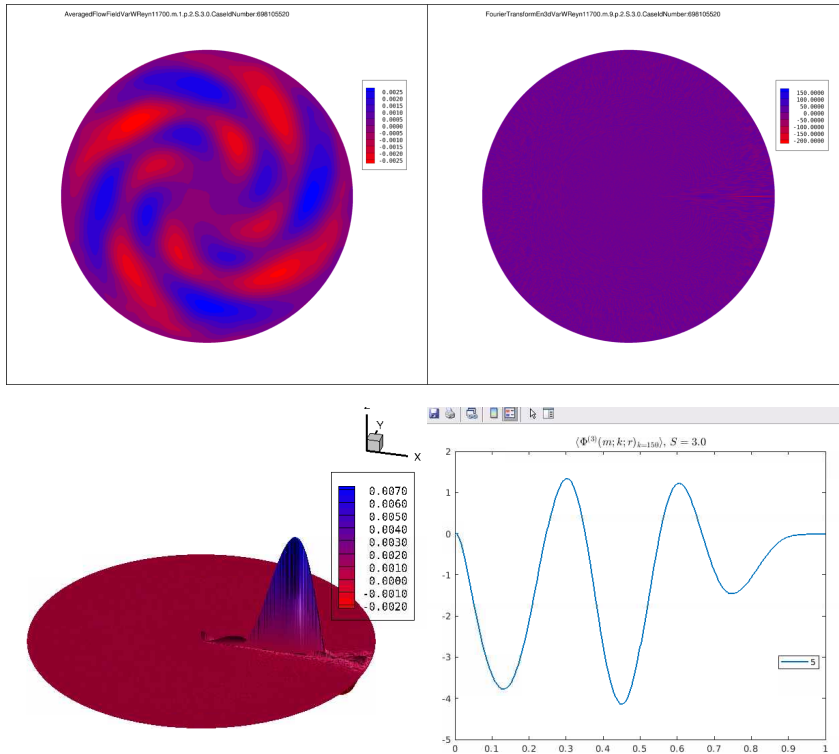


Figure 4.5: Derivation of POD projections

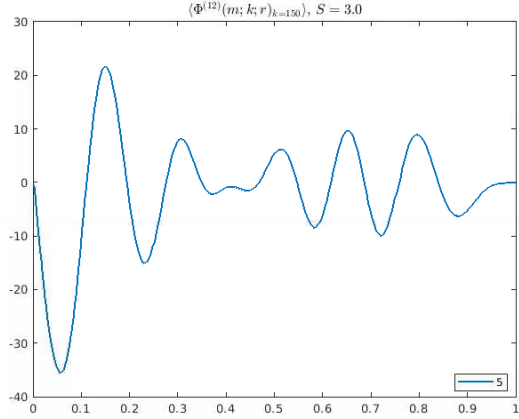
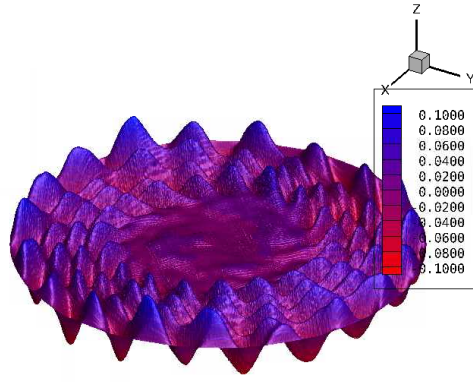


Figure 4.6: Arbitrary POD mode (here pictured:  $(n, m) = (12, 5)$  with  $S = 3$ ) is  $C^\infty$ . No windowing has been applied, and for most modes whose 2D POD projections are converged, no spectral leakage is present.

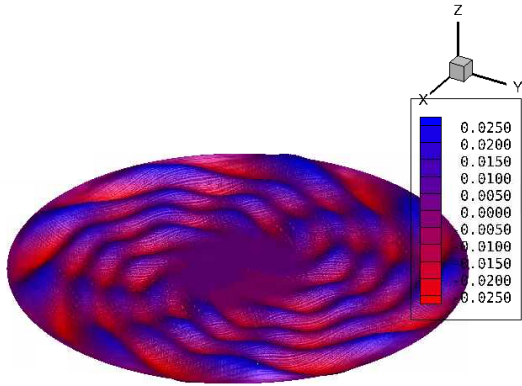
For all swirl numbers  $S = 0$  and  $S = 3$ , As shown in Figure 4.0.2, the modal profiles of all streamwise components have energy content closer to the pipe wall (at  $r = 0$ ). For non-zero swirl number  $S = 3$ , the amplitude appears to be more evenly distributed away from the wall for all azimuthal modes  $m$ . This result is in agreement with other reported findings, such as Feiz, Ould-Rouis, and Lauriat [24].

#### 4.0.4 Most Dominant Modes

This subsection shall give a graph of the most dominant azimuthal and POD modes. Based on this it is able to form the reduced order model (ROM). It is believed that the most azimuthal mode will be  $m \in [1, 3]$  for non-zero swirl numbers, as was the case for zero swirl, using Hellström and Smits [37] as a validation case.



(Above) Showing forth order mode with no rotation  $S=0$  showing larger amplitude and importance than (below) for the same mode with swirl  $S=3$



#### 4.0.5 Turbulent Statistics

This subsection shall compare classical turbulent statistic quantities such as TKE (turbulent kinetic energy) and Reynolds stress tensor results. It shall discuss momentum transport and a hypothesized reduction in skin friction, if seen, due to swirl. If low number azimuthal modes, such as  $m \in [0, 3]$  for POD modes  $\in [1, 2]$  have the largest energy (greatest eigenvalue  $\lambda$ ), then we can identify the mechanism that transports the flow away from the wall, and where closer to the pipe center the flow is transported to. This can be done very soon.

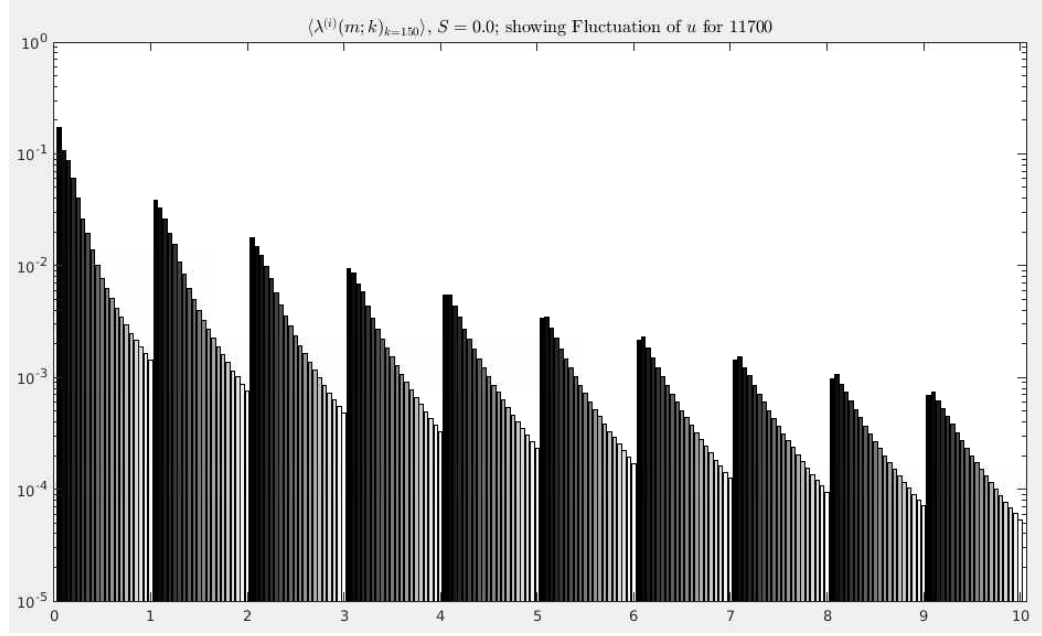
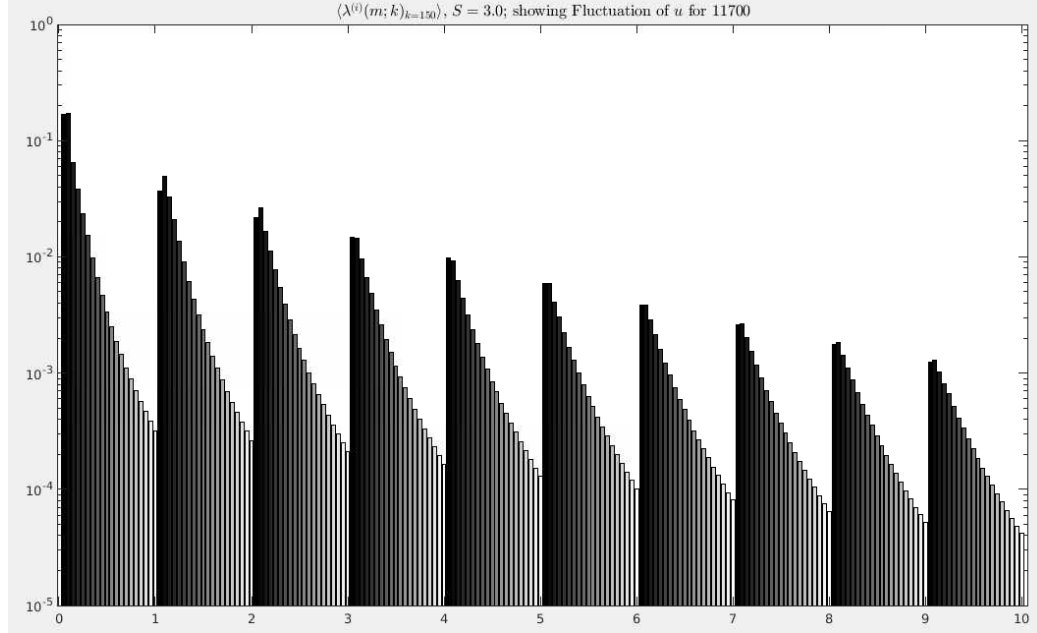


Figure 4.7: (top) The modal profiles of the streamwise component  $\langle \phi^{(1)} \rangle$  for  $S = 0.0$ . The modal profiles show the energy content in relation to the pipe wall  $r = 0$ . (bottom) Contour plots of the streamwise components of sample POD modes for  $m = \{5, 10, \dots, 30\}$  for  $n = 1$ . Note that since these modes are converged, and those we are then able to recover the modal profiles shown at (top).



#### 4.0.6 Reconstruction

When using POD for fluid dynamics, we start with a vector field,  $\mathbf{q}(\xi, t)$ , such as velocity. We subtract its average over time,  $\bar{\mathbf{q}}(\xi)$ , and then assume that the fluctuating part can be expressed as a sum of terms:

$$\mathbf{q}(\xi, t) - \bar{\mathbf{q}}(\xi) = \sum_j a_j \phi_j(\xi, t)$$

Here,  $\phi_j(\xi, t)$  are known as the modes, and  $a_j$  are the coefficients that scale these modes. The spatial coordinates are represented by  $\xi$ . This equation shows how the flow field can be represented using a series of basis functions,  $\phi_j(\xi, t)$ , which is similar to a Fourier series.

In the above POD approach, the goal is to find the best set of these basis functions to describe the data of the flow field by separating space and time, and focusing only on spatial modes, so that the velocity field reconstruction is given by,

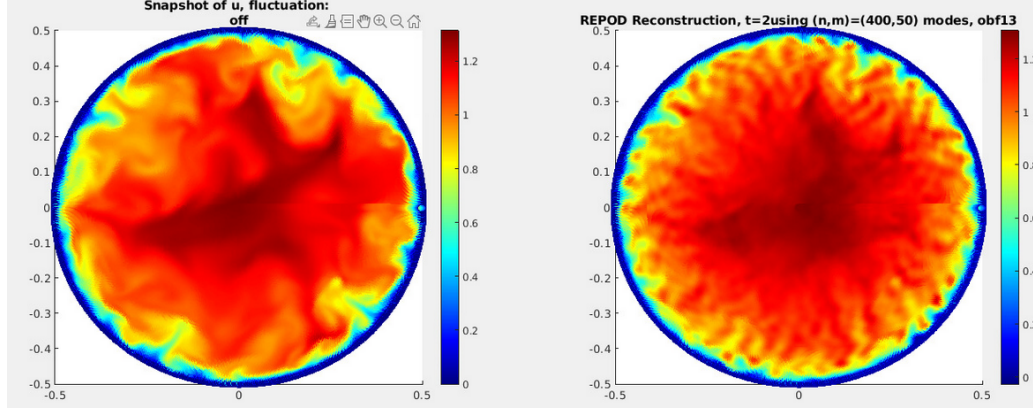


Figure 4.8: Reconstruction of a snapshot using 400 POD modes and 50 azimuthal modes.

$$q(\xi, t) - \bar{q}(\xi) = \sum_j \alpha_j(t) \Phi_j(\xi) \quad (4.4)$$

In performing reconstruction convergence appears to be monotonic, however, it must be verified that the FFT does not introduce artifacts, which for (eg  $Re=11,700$ ,  $S=0$ )  $m \approx 150$  azimuthal modes may be taken before artifacts appear. Reconstruction is another verification of the correctness of the POD procedure and code, along with (identities to be included).

## Chapter 5

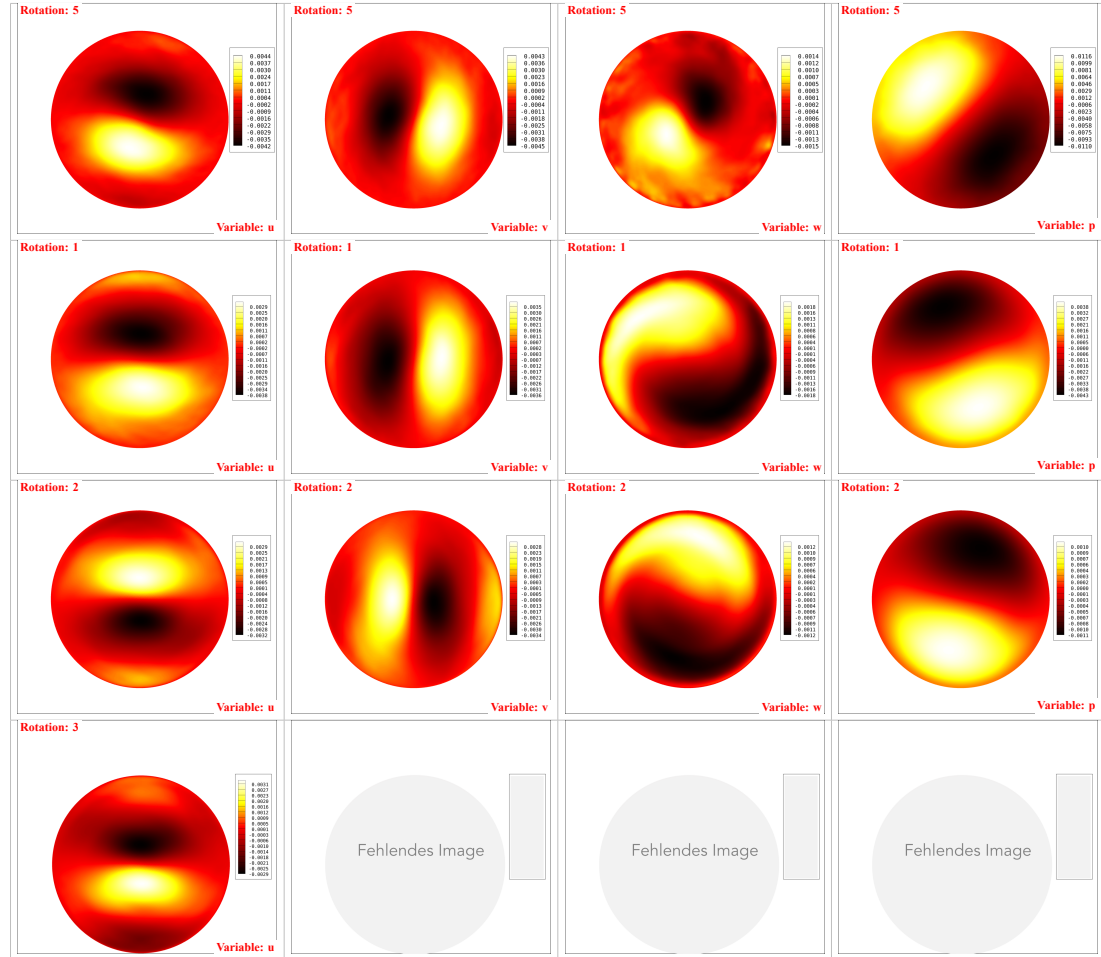
### Appendix to: Rotating Pipe POD Results

#### 5.1 POD Mode Projections

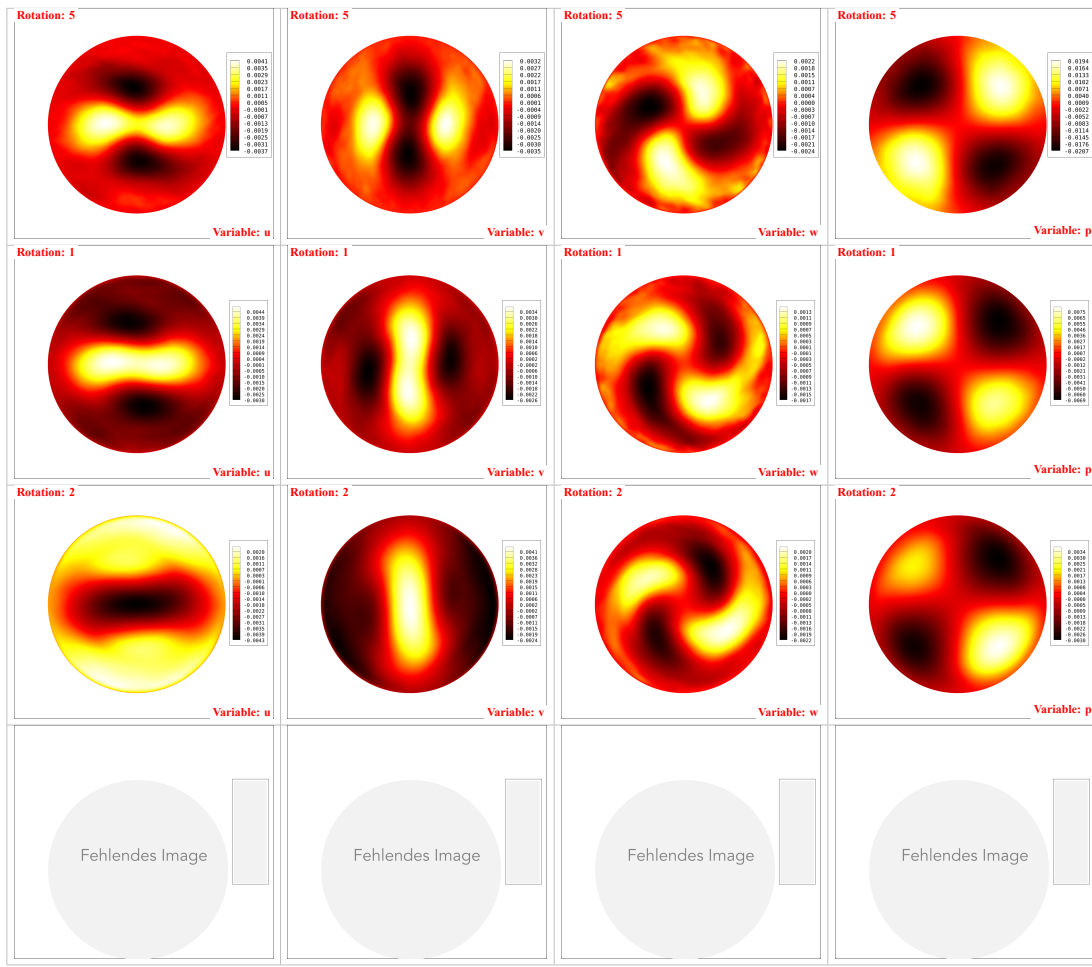
The following shows 2d POD projections for all flow fluctuations, for variables  $u = u_\theta, v = u_r, w = u_x$  and pressure  $p$  and  $S = \{0, 0.5, 1, 3\}$ .

Most projections are or can be converged.

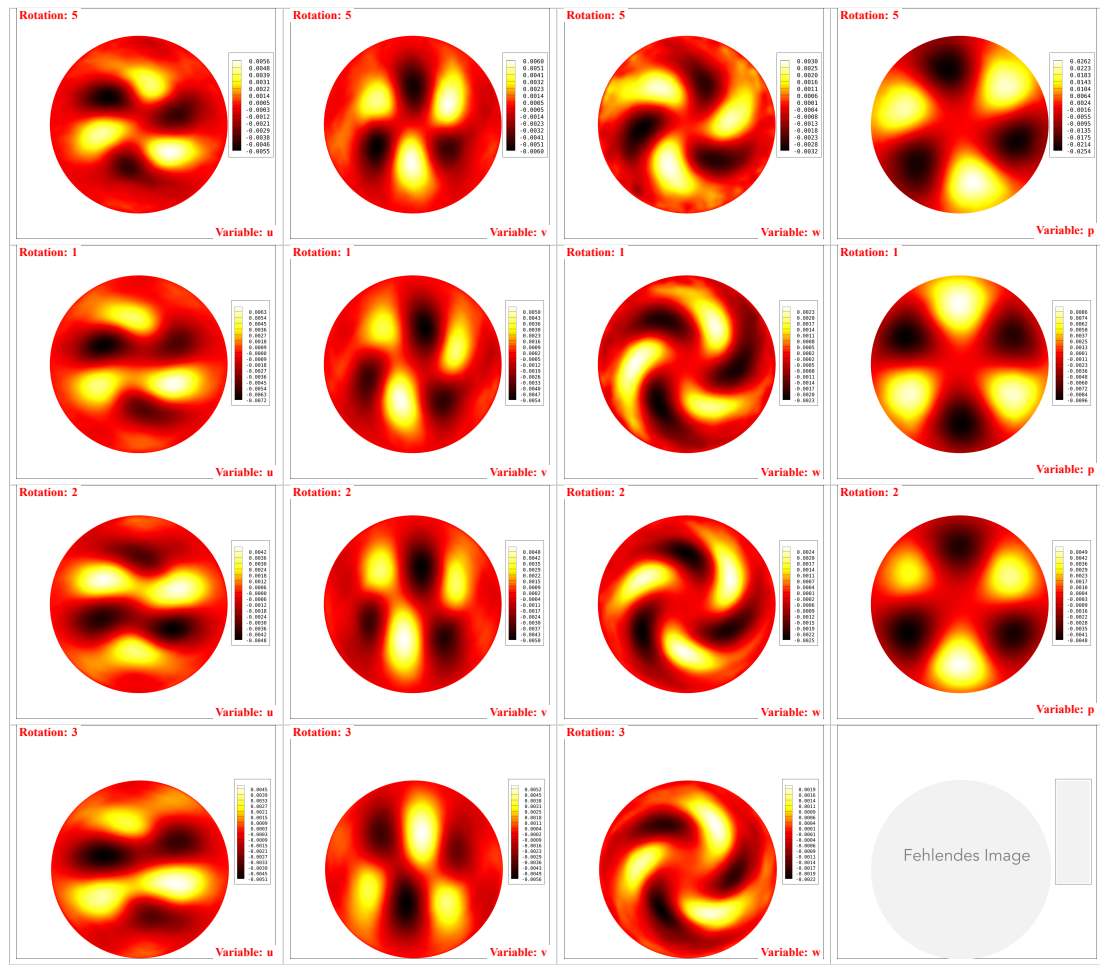
- $m = 1$



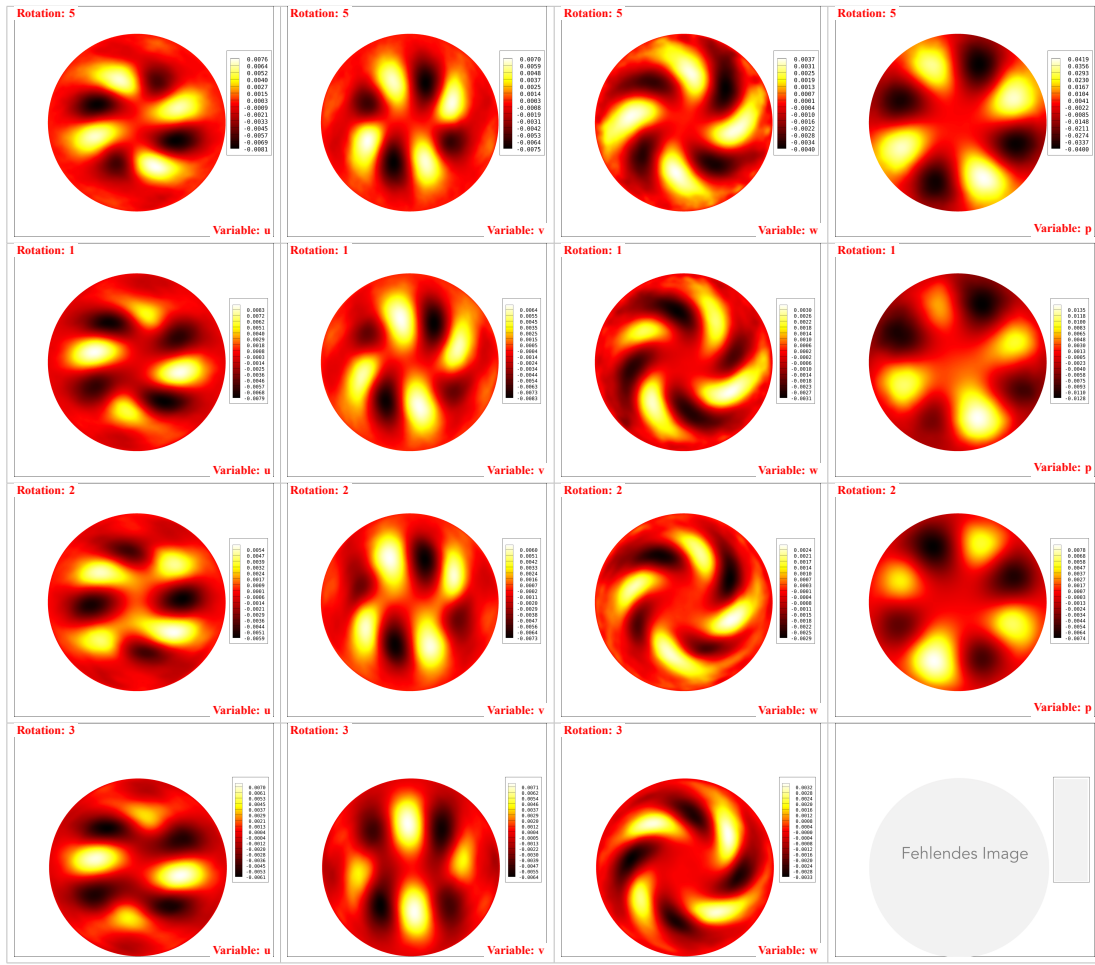
- $m = 2$



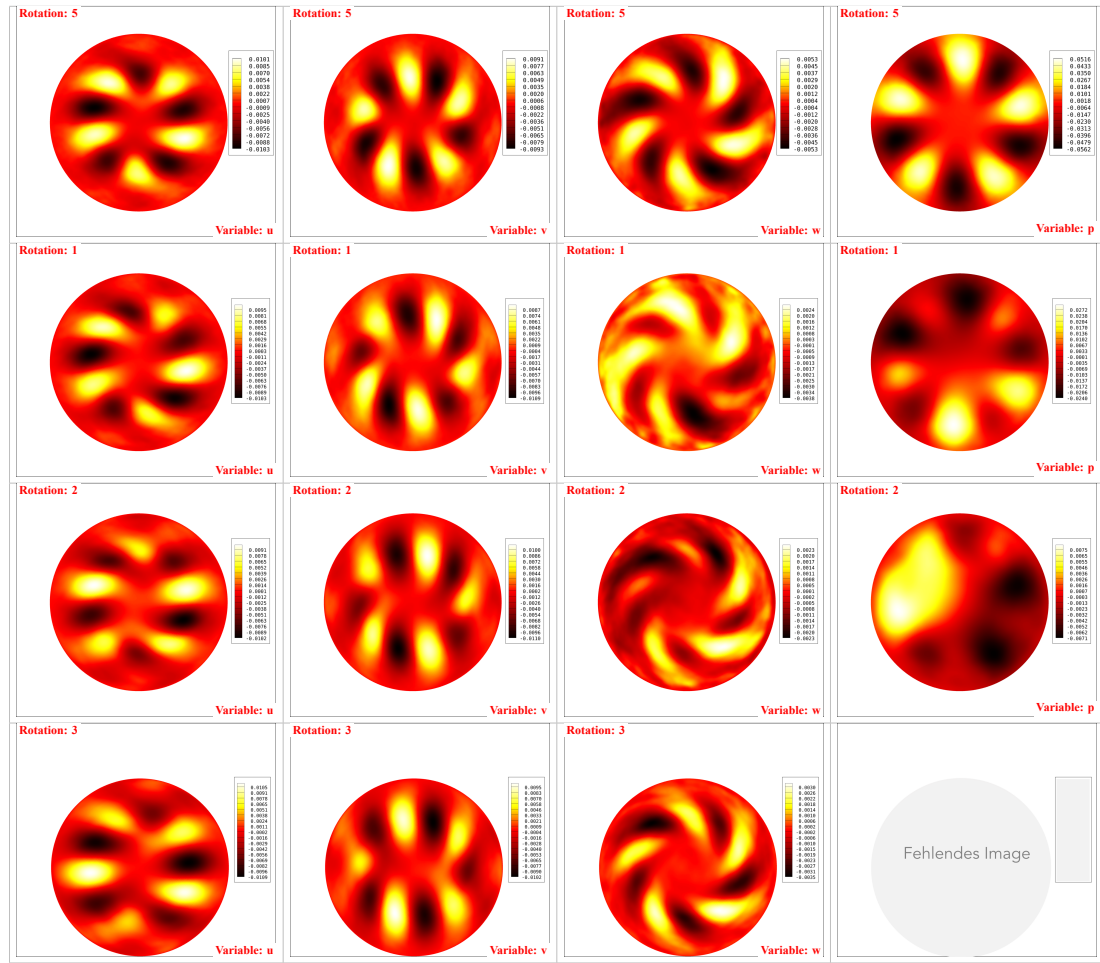
- $m = 3$



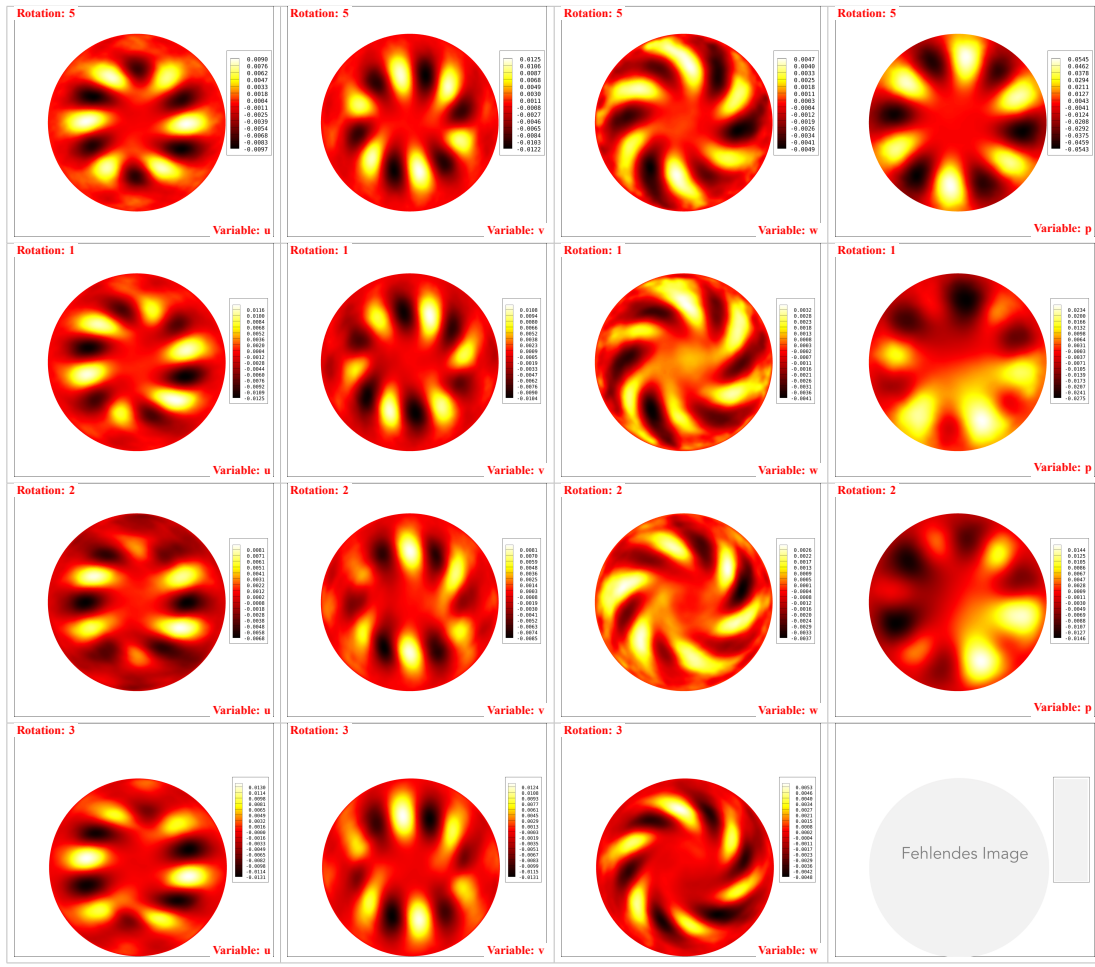
- $m = 4$



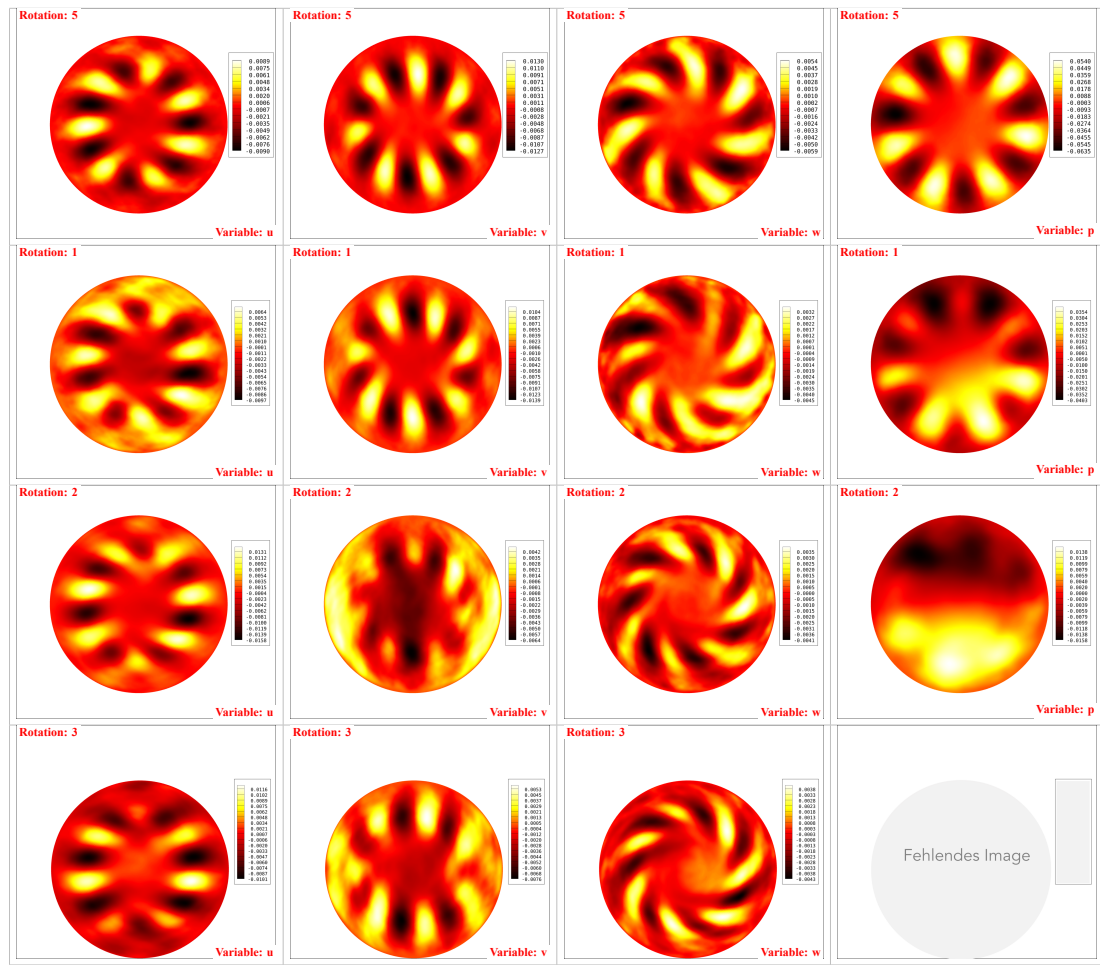
- $m = 5$



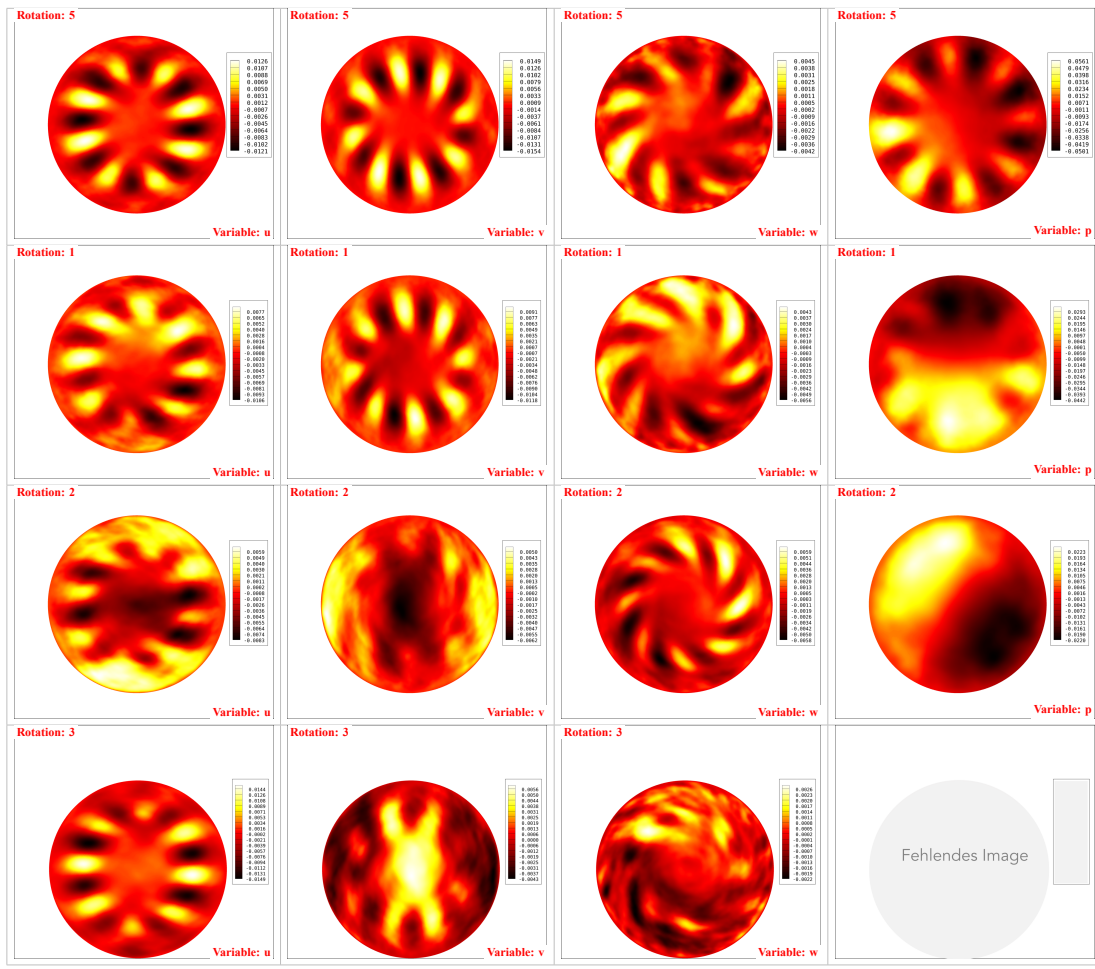
- $m = 6$



- $m = 7$



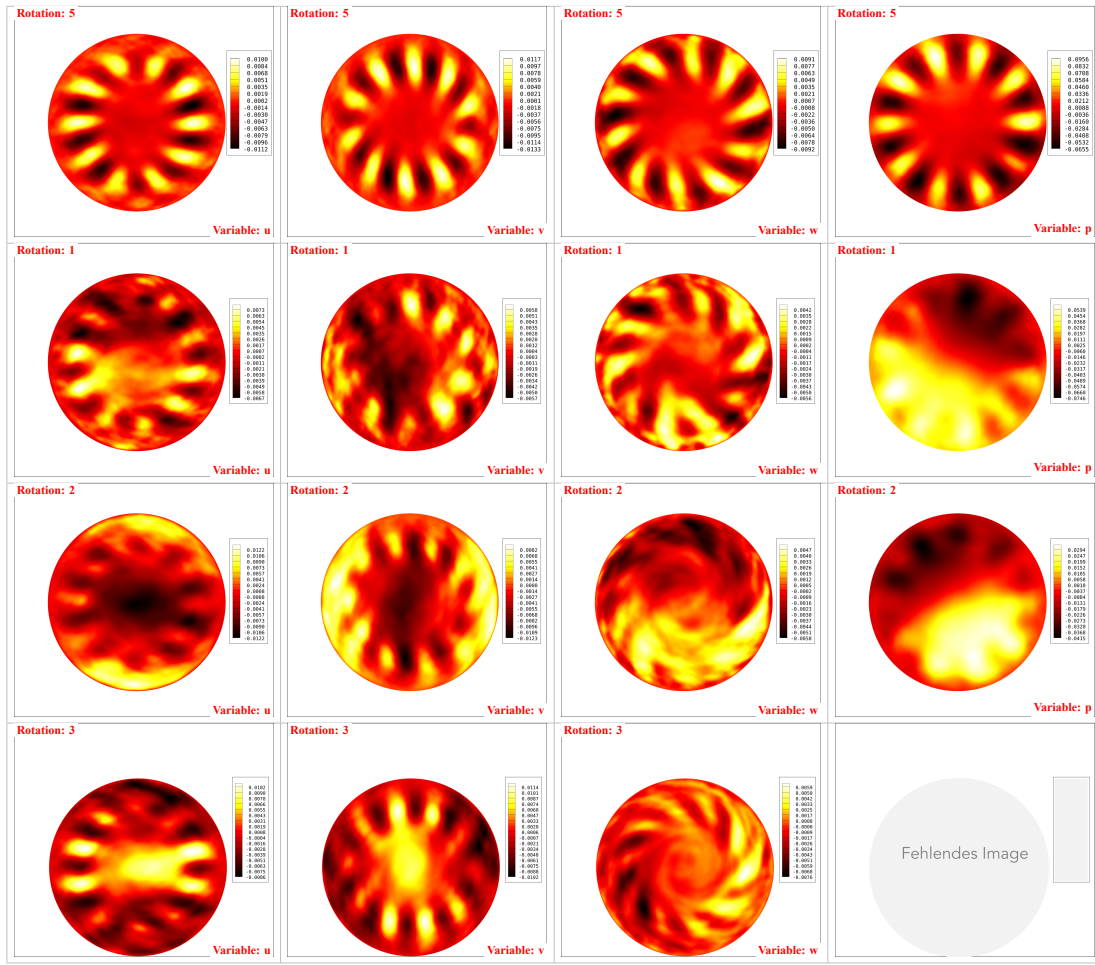
- $m = 8$



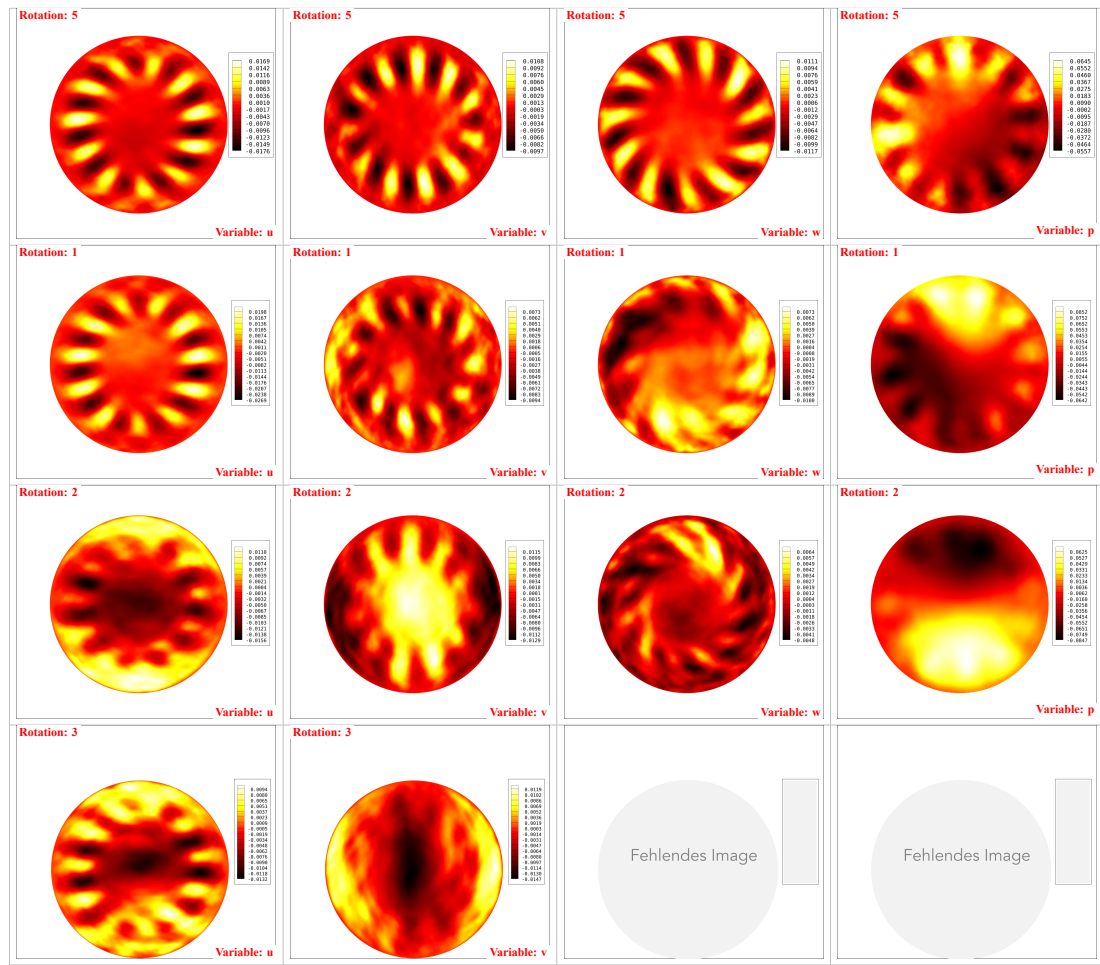
- $m = 9$



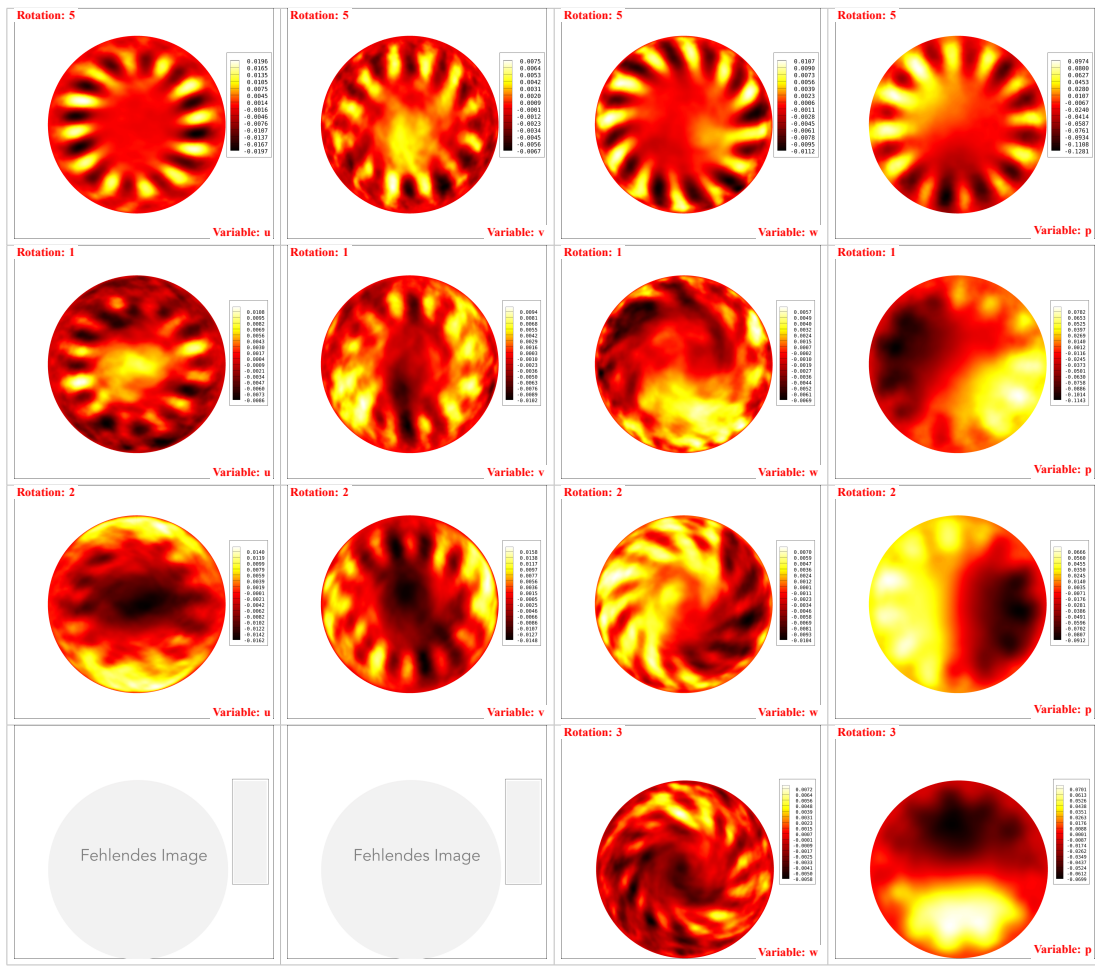
- $m = 10$



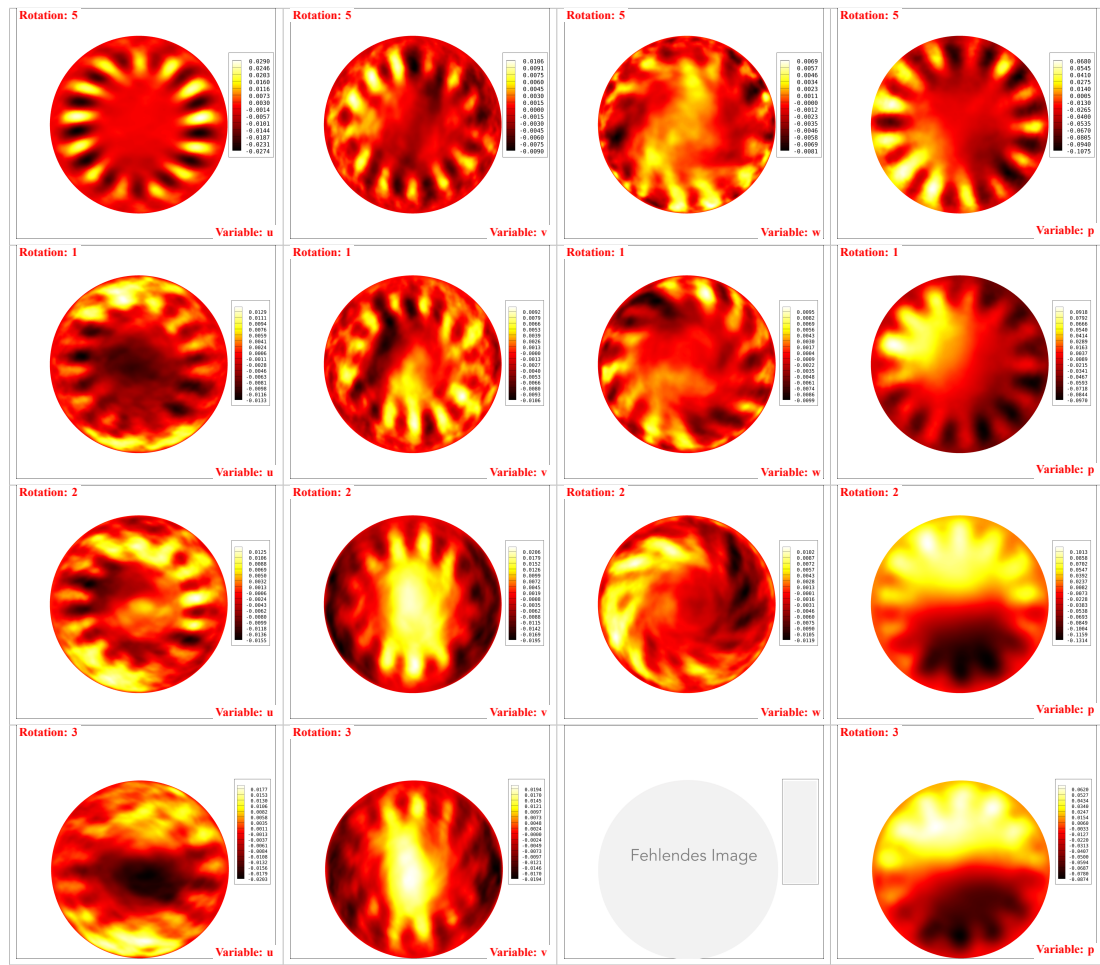
- $m = 11$



- $m = 12$



- $m = 13$





## Chapter 6

### Summary, Discussion, and Conclusions



## References

### 6.0.1 Coherent Structures

- [5] Nadine Aubry et al. “The dynamics of coherent structures in the wall region of a turbulent boundary layer”. In: *Journal of Fluid Mechanics* 192 (July 1988), pp. 115–173. ISSN: 1469-7645. DOI: 10.1017/s0022112088001818. URL: <http://dx.doi.org/10.1017/S0022112088001818>.
- [11] J. R. Baltzer, R. J. Adrian, and Xiaohua Wu. “Structural organization of large and very large scales in turbulent pipe flow simulation”. In: *Journal of Fluid Mechanics* 720 (Feb. 2013), pp. 236–279. ISSN: 1469-7645. DOI: 10.1017/jfm.2012.642. URL: <http://dx.doi.org/10.1017/jfm.2012.642>.
- [12] Gal Berkooz, Philip Holmes, and John L Lumley. “The proper orthogonal decomposition in the analysis of turbulent flows”. In: *Annual review of fluid mechanics* 25.1 (1993), pp. 539–575.
- [18] DAVID J. C. DENNIS and TIMOTHY B. NICKELS. “Experimental measurement of large-scale three-dimensional structures in a turbulent boundary layer. Part 2. Long structures”. In: *Journal of Fluid Mechanics* 673 (Mar. 2011), pp. 218–244. ISSN: 1469-7645. DOI: 10.1017/s0022112010006336. URL: <http://dx.doi.org/10.1017/S0022112010006336>.
- [33] Leo H. O. Hellström, Bharathram Ganapathisubramani, and Alexander J. Smits. “Coherent structures in transitional pipe flow”. In: *Physical Review Fluids* 1.2 (June 2016). ISSN: 2469-990X. DOI: 10.1103/physrevfluids.1.024403. URL: <http://dx.doi.org/10.1103/PhysRevFluids.1.024403>.
- [35] Leo H. O. Hellström, Aman Sinha, and Alexander J. Smits. “Visualizing the very-large-scale motions in turbulent pipe flow”. In: *Physics of Fluids* 23.1 (Jan. 2011), p. 011703. ISSN: 1089-7666. DOI: 10.1063/1.3533016. URL: <http://dx.doi.org/10.1063/1.3533016>.
- [43] Stephen J Kline et al. “The structure of turbulent boundary layers”. In: *Journal of Fluid Mechanics* 30.4 (1967), pp. 741–773.
- [52] Ivan Marusic and Jason P. Monty. “Attached Eddy Model of Wall Turbulence”. In: *Annual Review of Fluid Mechanics* 51.1 (Jan. 2019), pp. 49–74. ISSN: 1545-4479. DOI: 10.1146/annurev-fluid-010518-040427. URL: <http://dx.doi.org/10.1146/annurev-fluid-010518-040427>.
- [55] Parviz Moin and Robert D. Moser. “Characteristic-eddy decomposition of turbulence in a channel”. In: *Journal of Fluid Mechanics* 200 (Mar. 1989), pp. 471–509. ISSN: 1469-7645. DOI: 10.1017/s0022112089000741. URL: <http://dx.doi.org/10.1017/S0022112089000741>.
- [70] Stephen K Robinson. “Coherent motions in the turbulent boundary layer”. In: *Annual review of fluid mechanics* 23.1 (1991), pp. 601–639.
- [89] Jie Yao et al. “Direct numerical simulations of turbulent pipe flow up to  $Re_\tau \approx 5200$ ”. In: *Journal of Fluid Mechanics* 956 (Feb. 2023). ISSN: 1469-7645. DOI: 10.1017/jfm.2022.1013. URL: <http://dx.doi.org/10.1017/jfm.2022.1013>.

### 6.0.2 Rotating Pipes

- [4] Neil Ashton and Michael K. Stoellinger. “Computation of Turbulent Flow in a Rotating Pipe using the Elliptic Blending Reynolds Stress Model”. In: *46th AIAA Fluid Dynamics Conference* (June 2016). DOI: 10.2514/6.2016-3943. URL: <http://dx.doi.org/10.2514/6.2016-3943>.
- [14] C Brehm et al. “A numerical investigation of the effects of rotation on turbulent pipe flows”. In: *11th International Symposium on Turbulence and Shear Flow Phenomena (TSFP11)*. 2019 (cit. on p. 1).

- [23] Luca Facciolo. “A study on axially rotating pipe and swirling jet flows”. PhD thesis. KTH, 2006.
- [24] A. A. Feiz, M. Ould-Rouis, and G. Lauriat. “Turbulence Statistics in a Fully Developed Rotating Pipe Flow”. In: *Journal of Enhanced Heat Transfer* 12.3 (2005), pp. 273–288. ISSN: 1065-5131. DOI: 10.1615/jenhheattransf.v12.i3.50. URL: <http://dx.doi.org/10.1615/JEnhHeatTransf.v12.i3.50> (cit. on pp. 2, 17).
- [30] Harvey Philip Greenspan. *The Theory of Rotating Fluids*. 1968.
- [37] Leo HO Hellström and Alexander J Smits. “Structure identification in pipe flow using proper orthogonal decomposition”. In: *Philosophical Transactions of the Royal Society A: Mathematical, Physical and Engineering Sciences* (2017) (cit. on pp. 11, 14, 17).
- [40] Shigeki Imao, Motoyuki Itoh, and Takeyoshi Harada. “Turbulent characteristics of the flow in an axially rotating pipe”. In: *International Journal of Heat and Fluid Flow* 17.5 (Oct. 1996), pp. 444–451. ISSN: 0142-727X. DOI: 10.1016/0142-727X(96)00057-4. URL: [http://dx.doi.org/10.1016/0142-727X\(96\)00057-4](http://dx.doi.org/10.1016/0142-727X(96)00057-4) (cit. on p. 1).
- [42] Koji Kikuyama et al. “Flow in an Axially Rotating Pipe: A calculation of flow in the saturated region”. In: *Bulletin of JSME* 26.214 (1983), pp. 506–513. ISSN: 1881-1426. DOI: 10.1299/jsme1958.26.506. URL: <http://dx.doi.org/10.1299/jsme1958.26.506> (cit. on pp. 1, 11).
- [56] R Narasimha and KR Sreenivasan. “Relaminarization of fluid flows”. In: *Advances in applied mechanics* 19 (1979), pp. 221–309.
- [61] Orlandi and Fatica. “Direct simulations of turbulent flow in a pipe rotating about its axis”. In: *Journal of Fluid Mechanics* 343 (July 1997), pp. 43–72. DOI: 10.1017/s0022112097005715. URL: <http://dx.doi.org/10.1017/S0022112097005715> (cit. on p. 1).
- [69] G. Reich and H. Beer. “Fluid flow and heat transfer in an axially rotating pipe—I. Effect of rotation on turbulent pipe flow”. In: *International Journal of Heat and Mass Transfer* 32.3 (Mar. 1989), pp. 551–562. ISSN: 0017-9310. DOI: 10.1016/0017-9310(89)90143-9. URL: [http://dx.doi.org/10.1016/0017-9310\(89\)90143-9](http://dx.doi.org/10.1016/0017-9310(89)90143-9) (cit. on p. 2).
- [85] A. White. “Flow of a Fluid in an Axially Rotating Pipe”. In: *Journal of Mechanical Engineering Science* 6.1 (Mar. 1964), pp. 47–52. ISSN: 2058-3389. DOI: 10.1243/jmes\_jour\_1964\_006\_010\_02. URL: [http://dx.doi.org/10.1243/JMES\\_JOUR\\_1964\\_006\\_010\\_02](http://dx.doi.org/10.1243/JMES_JOUR_1964_006_010_02) (cit. on p. 1).

### 6.0.3 Turbulent Flows

- [1] Ronald J Adrian, Carl D Meinhart, and Christopher D Tomkins. “Vortex organization in the outer region of the turbulent boundary layer”. In: *Journal of fluid Mechanics* 422 (2000), pp. 1–54.
- [2] C.D. Argyropoulos and N.C. Markatos. “Recent advances on the numerical modelling of turbulent flows”. In: *Applied Mathematical Modelling* 39.2 (Jan. 2015). dns of turbulent pipe flows p 716; good review paper!, p. 716. ISSN: 0307-904X. DOI: 10.1016/j.apm.2014.07.001. URL: <http://dx.doi.org/10.1016/j.apm.2014.07.001>.
- [7] SEAN C. C. Bailey et al. “Azimuthal structure of turbulence in high Reynolds number pipe flow”. In: *Journal of Fluid Mechanics* 615 (Nov. 2008). has correlation coefficient on page 127, pp. 121–138. ISSN: 1469-7645. DOI: 10.1017/s0022112008003492.
- [9] Henry P. Bakewell. “Viscous Sublayer and Adjacent Wall Region in Turbulent Pipe Flow”. In: *Physics of Fluids* 10.9 (1967), p. 1880. ISSN: 0031-9171. DOI: 10.1063/1.1762382. URL: <http://dx.doi.org/10.1063/1.1762382>.
- [13] Peter Bradshaw and George P Huang. “The law of the wall in turbulent flow”. In: *Proceedings of the Royal Society of London. Series A: Mathematical and Physical Sciences* 451.1941 (1995), pp. 165–188.
- [16] Peter Davidson. *Turbulence: an introduction for scientists and engineers*. Oxford university press, 2015.
- [38] M. Hultmark et al. “Turbulent Pipe Flow at Extreme Reynolds Numbers”. In: *Physical Review Letters* 108.9 (Feb. 2012). ISSN: 1079-7114. DOI: 10.1103/physrevlett.108.094501. URL: <http://dx.doi.org/10.1103/PhysRevLett.108.094501>.

- [44] Andrei Nikolaevich Kolmogorov. “The local structure of turbulence in incompressible viscous fluid for very large Reynolds numbers”. In: *Proceedings of the Royal Society of London. Series A: Mathematical and Physical Sciences* (1941) (cit. on p. 1).
- [50] I. Marusic et al. “Wall-bounded turbulent flows at high Reynolds numbers: Recent advances and key issues”. In: *Physics of Fluids* 22.6 (June 2010). Motivation why we care about wall turbulence and coherent structures, p. 065103. ISSN: 1089-7666. DOI: 10.1063/1.3453711. URL: <http://dx.doi.org/10.1063/1.3453711>.
- [53] B. J. McKEON and A. S. SHARMA. “A critical-layer framework for turbulent pipe flow”. In: *Journal of Fluid Mechanics* 658 (July 2010), pp. 336–382. ISSN: 1469-7645. DOI: 10.1017/s002211201000176x. URL: <http://dx.doi.org/10.1017/S002211201000176X>.
- [68] Tomás Chacón Rebollo and Roger Lewandowski. *Mathematical and numerical foundations of turbulence models and applications*. Springer, 2014.
- [72] Pierre Sagaut and Claude Cambon. *Homogeneous Turbulence Dynamics*. Springer, 2008.
- [76] L. Sirovich, K. S. Ball, and L. R. Keefe. “Plane waves and structures in turbulent channel flow”. In: *Physics of Fluids A: Fluid Dynamics* 2.12 (Dec. 1990), pp. 2217–2226. ISSN: 0899-8213. DOI: 10.1063/1.857808. URL: <http://dx.doi.org/10.1063/1.857808>.
- [77] Lawrence Sirovich. “Turbulence and the dynamics of coherent structures. I. Coherent structures”. In: *Quarterly of applied mathematics* 45.3 (1987), pp. 561–571.
- [79] B.M. Sumer and D.R. Fuhrman. *Turbulence In Coastal And Civil Engineering*. Advanced Series On Ocean Engineering. World Scientific Publishing Company, 2020, pp. 184–. ISBN: 9789813234321. URL: <https://books.google.com/books?id=ztLkDwAAQBAJ>.
- [81] AAR Townsend. *The structure of turbulent shear flow*. Cambridge university press, 1980.
- [86] WW Willmarth and SS Lu. “Structure of the Reynolds stress near the wall”. In: *Journal of Fluid Mechanics* 55.1 (1972), pp. 65–92.

#### 6.0.4 Classical POD

- [8] Sean CC Bailey and Alexander J Smits. “Experimental investigation of the structure of large-and very-large-scale motions in turbulent pipe flow”. In: *Journal of Fluid Mechanics* 651 (2010), pp. 339–356.
- [26] Stephan Gamard et al. “Application of a “slice” proper orthogonal decomposition to the far field of an axisymmetric turbulent jet”. In: *Physics of Fluids* 14.7 (2002), p. 2515. ISSN: 1070-6631. DOI: 10.1063/1.1471875. URL: <http://dx.doi.org/10.1063/1.1471875>.
- [32] Leo Hellstroem. “Coherent Structures in Turbulent Pipe Flow”. PhD thesis. Princeton University, 2015. URL: <https://drive.google.com/file/d/1gPC02JtRyHa9cdRU0ZwoQfkCrJLwDfYV/view?usp=sharing>.
- [34] Leo H. O. Hellström, Ivan Marusic, and Alexander J. Smits. “Self-similarity of the large-scale motions in turbulent pipe flow”. In: *Journal of Fluid Mechanics* 792 (Mar. 2016). ISSN: 1469-7645. DOI: 10.1017/jfm.2016.100. URL: <http://dx.doi.org/10.1017/jfm.2016.100> (cit. on pp. 11, 12, 14).
- [58] Bernd R. Noack. “Turbulence, Coherent Structures, Dynamical Systems and Symmetry”. In: *AIAA Journal* 51.12 (Dec. 2013), pp. 2991–2991. ISSN: 1533-385X. DOI: 10.2514/1.j052557. URL: <http://dx.doi.org/10.2514/1.J052557>.

#### 6.0.5 Spectral Analysis

- [66] Markus Raffel, Christian E Willert, Jürgen Kompenhans, et al. *Particle image velocimetry: a practical guide*. Vol. 2. discussion of phase shift of the imaginary part being equivalent to the real part Phi POD mode. Springer, 1998.
- [82] Murat Tutkun, Peter B. V. Johansson, and William K. George. “Three-Component Vectorial Proper Orthogonal Decomposition of Axisymmetric Wake Behind a Disk”. In: *AIAA Journal* 46.5 (2008). DOI: 10.2514/1.31074. URL: <https://sci-hub.hkvisa.net/10.2514/1.31074>.

- [88] Xiaohua Wu and Parviz Moin. “A direct numerical simulation study on the mean velocity characteristics in turbulent pipe flow”. In: *Journal of Fluid Mechanics* 608 (July 2008), pp. 81–112. ISSN: 1469-7645. DOI: 10.1017/s0022112008002085. URL: <http://dx.doi.org/10.1017/s0022112008002085>.

## 6.0.6 NEK5000

- [22] George K. El Khoury et al. “Direct Numerical Simulation of Turbulent Pipe Flow at Moderately High Reynolds Numbers”. In: *Flow, Turbulence and Combustion* 91.3 (July 2013), pp. 475–495. ISSN: 1573-1987. DOI: 10.1007/s10494-013-9482-8. URL: <http://dx.doi.org/10.1007/s10494-013-9482-8>.
- [73] Sandip Saha, Pankaj Biswas, and Sujit Nath. “A review on spectral element solver Nek5000”. In: *AIP Conference Proceedings* (2021). ISSN: 0094-243X. DOI: 10.1063/5.0045709. URL: <http://dx.doi.org/10.1063/5.0045709>.
- [83] Ricardo Vinuesa et al. “Aspect ratio effects in turbulent duct flows studied through direct numerical simulation”. In: *Journal of Turbulence* 15.10 (July 2014), pp. 677–706. ISSN: 1468-5248. DOI: 10.1080/14685248.2014.925623. URL: <http://dx.doi.org/10.1080/14685248.2014.925623>.